

Plasmonic Nanostructure Engineering with Shadow Growth

Jang-Hwan Han, Doeun Kim, Juhwan Kim, Gyurin Kim, Peer Fischer,*
and Hyeon-Ho Jeong*

Physical shadow growth is a vacuum deposition technique that permits a wide variety of 3D-shaped nanoparticles and structures to be fabricated from a large library of materials. Recent advances in the control of the shadow effect at the nanoscale expand the scope of nanomaterials from spherical nanoparticles to complex 3D shaped hybrid nanoparticles and structures. In particular, plasmonically active nanomaterials can be engineered in their shape and material composition so that they exhibit unique physical and chemical properties. Here, the recent progress in the development of shadow growth techniques to realize hybrid plasmonic nanomaterials is discussed. The review describes how fabrication permits the material response to be engineered and highlights novel functions. Potential fields of application with a focus on photonic devices, biomedical, and chiral spectroscopic applications are discussed.

As a result, photons are not only absorbed and converted to phonons (and ultimately heat),^[8–11] but they are also strongly scattered. Stable colors can thus be generated in metallic nanostructures that differ from those of the corresponding bulk materials.^[12] Crucially, structural control of nanoscale features including shape and symmetry,^[7,13,14] material composition,^[13–17] as well as the overall arrangement within an ensemble^[6,14] or array,^[18,19] determines the exact nature of the plasmonic response. This is successfully exploited in diverse applications.

Solution chemistry has been widely used to grow a range of highly symmetric nanoparticles (spherical, rod-shaped, pyramidal, etc.).^[20–23] Energetically, structures with high symmetry are generally favored, so that there are no facile wet methods to synthesize complex 3D-shaped hybrid metallic nanoparticles of low symmetry.^[24,25] One notable exception are chiral gold nanoparticles, including triangular nanorings,^[26] helicoids,^[27,28] and spirals,^[29,30] that have been synthesized using a two-step growth method consisting of the synthesis of highly symmetric gold nanoparticles followed by further growth in the presence of chiral molecules.^[28] Apart from this example, it is challenging to obtain more complex 3D shapes and to freely vary the material composition.^[31,32] In contrast, physical methods that are often restricted to the growth on a substrate, offer more freedom in the choice of materials and geometry. Often electron-/ion-beam-lithography is used to realize diverse 2D and 2.5D plasmonic structures. For instance, plasmonic structures such as bow-tie nanoantennas,^[33,34] metamolecular structures,^[35–37] and chiral gammadions^[38,39] have been fabricated.

To obtain truly 3D structures, physical shadow growth techniques are superior, as they permit the control of the material composition and the 3D geometry at the wafer-scale. In conjunction with nanoscale shadowing, plasmonic nanomaterials can be fabricated,^[40,41] including core/shell, patchy, Janus structures,^[42–50] low-symmetry shapes (zigzag, hook, crescent, and helix),^[25,43,51,52] and a large number of hybrid structures with tailored material compositions (e.g., Au–Fe,^[53] Ag–Ti,^[54] Ag–MgF₂,^[55] and Ag–Cu^[56]). These structures are difficult to achieve with any other growth method. Moreover, physical shadowing can also be used to obtain periodic arrangements of nanostructures.^[25,40,57,58] After removal from the substrate, for example, through sonication, one can also obtain suspensions of nanocolloids.^[25] In contrast to wet synthesis, the nanostructures are grown without stabilizing ligands and can thus be more easily functionalized. Physical growth yields superior


1. Introduction

Plasmonic nanomaterials are structures made of metals (e.g., gold, silver, copper, aluminum, and magnesium) with a characteristic size that is smaller than the wavelength of visible light.^[1–4] Key features that distinguish plasmonic from many other nanomaterials are the unique optical properties resulting from strong, resonant light–matter interactions. Known as local surface plasmon resonance (LSPR),^[3,5–7] this phenomenon involves the coherent oscillation and excitation of free electrons in the bulk of nanostructures upon irradiation of light. The optical near-field is strongly enhanced, which can be exploited for interactions with the medium surrounding a nanoparticle.

J.-H. Han, D. Kim, J. Kim, G. Kim, H.-H. Jeong
School of Electrical Engineering and Computer Science
Gwangju Institute of Science and Technology
Gwangju 61005, Republic of Korea
E-mail: jeong323@gist.ac.kr

P. Fischer
Max Planck Institute for Intelligent Systems
Heisenbergstr. 3, 70569 Stuttgart, Germany
E-mail: fischer@is.mpg.de

P. Fischer
Institute of Physical Chemistry
University of Stuttgart
Pfaffenwaldring 55, 70569 Stuttgart, Germany

 The ORCID identification number(s) for the author(s) of this article can be found under <https://doi.org/10.1002/adma.202107917>.

© 2022 The Authors. Advanced Materials published by Wiley-VCH GmbH. This is an open access article under the terms of the Creative Commons Attribution License, which permits use, distribution and reproduction in any medium, provided the original work is properly cited.

DOI: 10.1002/adma.202107917

optical properties that enable single-particle linear and non-linear chiroptical scattering probes,^[59,60] and are simpler to integrate with photonic devices.^[61,62] They can also be used to grow structures for biomedical micro/nanorobotics.^[63,64]

Here, we highlight recent developments in the physical shadow growth of complex hybrid plasmonic nanomaterials. We describe structures that show increasingly higher complexity, that is, lower symmetry and several tuned parameters for selected target applications. This review highlights some unique properties exhibited by shadow-grown plasmonic 3D nanomaterials that can typically not be obtained with other fabrication strategies. Examples include single particle chiroptical spectroscopy and self-propelling nanomotors for potential biomedical applications.

2. Physical Shadow Growth for Plasmonics

Nanomaterials in the subwavelength regime of visible light, that is, 10–100 nm in size, possess a LSPR. The electric dipole resonance dominates and distinct plasmonic colors are observed.^[3,5] When the size of the nanomaterial is smaller than 10 nm, the mean free path of the oscillating electrons can be longer than the dimension of the nanomaterial, resulting in quantum effects (see refs. [65, 66] for quantum plasmonics). Nanostructures that have dimensions larger than 100 nm typically exhibit higher-order resonance modes and radiation damping effects.^[67,68] Thus, depending on the desired application, at least one dimension should be greater than 10 nm and smaller than a few hundred nm to permit the excitation of a LSPR.

2.1. Local Surface Plasmon Resonance

The electric field of a light wave can penetrate metallic nanoparticles. Depending on the metal there is a resonant frequency

where the light wave can excite collective oscillations of electrons, which is known as LSPR and accompanies strong optical near-field enhancement on the surface of the plasmonic nanomaterials (**Figure 1**). In addition, one observes optical absorption of the incident photons. These are converted into phonons, which are the source of heat or acoustic waves. In addition, strong scattering takes place, where the nanoparticle reradiates at the incident frequency. The sum of these two processes is known as extinction (e.g., a nanosphere's extinction spectrum can be seen in the top panel of **Figure 1b**), E , expressed as,^[69,70]

$$E \propto \frac{\epsilon_i}{(\epsilon_r + \chi n^2)^2 + \epsilon_i^2} \quad (1)$$

where ϵ_r and ϵ_i are the real and imaginary terms of the metal's dielectric constant, χ is a shape factor of the metal nanoparticle, n is the refractive index of the medium surrounding the nanoparticle, λ is the wavelength of light. LSPR occurs when E becomes maximal, which defines the resonance condition:

$$\epsilon_r(\lambda^*) = -\chi n^2 \quad (2)$$

Equations (1) and (2) clearly show that the LSPR resonance wavelength λ^* is a function of the metal nanoparticle's shape factor χ , its effective dielectric function (material composition) ϵ_r , and the nature of the surrounding medium n . Nanomaterials can thus be fabricated to show LSPR bands anywhere in the visible spectrum, which is exploited in applications such as sensing,^[3,71–73] imaging,^[5,74,75] actuation,^[53,76] and display technologies.^[77,78] Advances in nanofabrication including in physical shadow growth techniques continuously extends the possible range for which the LSPR can be engineered. Here, we highlight such recent achievements (**Figure 1a**). Although the resonance condition in Equation (2) cannot fully describe complex geometries (e.g., chiral particles, the bottom panel of **Figure 1b**) and optical interactions (e.g., coupled systems, the

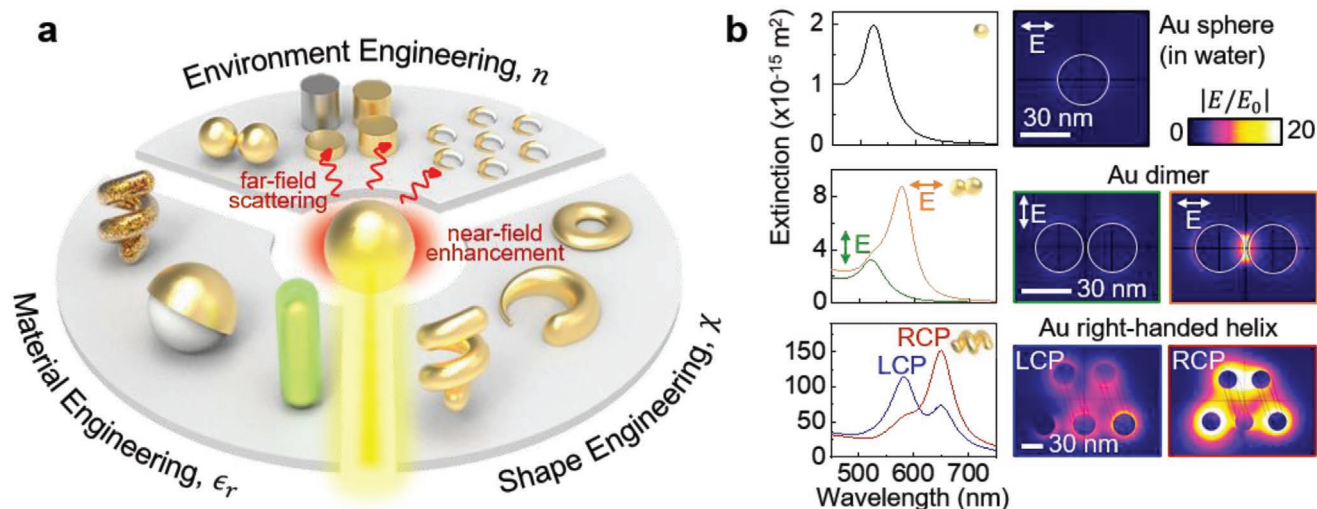


Figure 1. Hybrid plasmonic nanoparticles. a) Examples of plasmonic nanoparticles grown by physical vapor shadow growth methods. b) Numerical simulation of LSPR signals (left) and optical field enhancements (right) of: (top) Au sphere (diameter 30 nm), (middle) two representative examples of hybrid nanoparticles, including the optical near-field coupled dimer (diameter 30 nm, gap 2 nm), and (bottom) a chiral helix (minor radius 15 nm, major radius 35 nm, pitch 55 nm) in water (with respectively, LCP: left circularly polarized excitation, and RCP: right circularly polarized excitation).

middle panel of Figure 1b), it is nevertheless a helpful guide. It permits plasmonic nanomaterials to be categorized and we thus use it to discuss specific examples where: (i) χ , the shape is engineered: LSPR from simple sphere to complex shapes, including low symmetric and chiral structures. We also provide examples (ii) where the ϵ_r of a material is engineered: plasmonic alloys with functional materials (e.g., magnetic,^[44,53,79] catalytic,^[80,81] and phase change materials^[82,83]); and finally where the arrangement and coupling of nanoparticles are engineered, which affect (iii) n , the environment: near-field gap resonances and far-field lattice coupling.

2.2. Vacuum Growth for Nanomaterials

For the fabrication of nanomaterials, we here focus on vacuum growth schemes, which can be categorized into two main groups: chemical vapor deposition (CVD) and physical vapor deposition (PVD). CVD utilizes chemical reactions and the growth of gaseous precursors that interact with a surface at high temperatures, resulting in uniform clean thin films.^[84–87] This scheme has been largely advanced for growing low dimensional and atomically flat materials, viz. 2D materials.^[87–91] Recent optimization in the initial growth temperature (restricting between 1000 and 1030 K) leads to the growth of large area fold-free single-crystal monolayer graphene films.^[92] This is an exciting research domain with potential for flexible/wearable transparent electrode materials^[93–95] and optoelectronic devices.^[91,96,97] However, this scheme is incompatible with metals and metal alloys.

In contrast, PVD can be used to grow thin films from a large number of materials, including metals, semiconductors, insulators, magnetic materials, as well as alloys thereof. Vapors of atoms or molecules are generated in vacuum with thermal or electron-beam assisted heating. These travel directionally and deposit on the target substrate to form adatoms.^[25,40,58,98] The mobility of the adatoms and their interaction with the surface as well as other adatoms determines the structural profile that is formed.^[99] If the vapor flux is incident along the surface normal, the entire substrate is coated with a continuous thin film. In combination with lithographic techniques, normal-incidence PVD can be used to grow planar (2.5D) plasmonic structures with nanoscale precision, including for instance bow-tie nanoantennas,^[33,34] metamolecular structures,^[35–37] and 2D-chiral gammadians.^[38,39] However, this approach does not lend itself for wafer-scale or truly 3D processing.

Remarkably, only a slight modification is required to obtain wafer-scale grown 3D nanoparticles with PVD. When the substrate is angled such that the vapor flux is no longer along the surface normal, but almost orthogonal, that is, at an oblique or glancing angle along the surface plane (Figure 2a), then shadowing gives rise to nanostructuring. Any structure present on the substrate, even as simple as a few random clusters of atoms, serves as a seed onto which material preferentially deposits leaving an area free from deposits in the shadow of the seed.^[40,98,100] If there are many such seed particles on the surface, the growth leads to an array of slanted columnar structures on top of seeds (e.g., Figure 2d[iii]). First investigated in 1950,^[101] this growth has later been termed oblique angle deposition (OAD).^[102] In 1959, the first azimuthal rotation of the

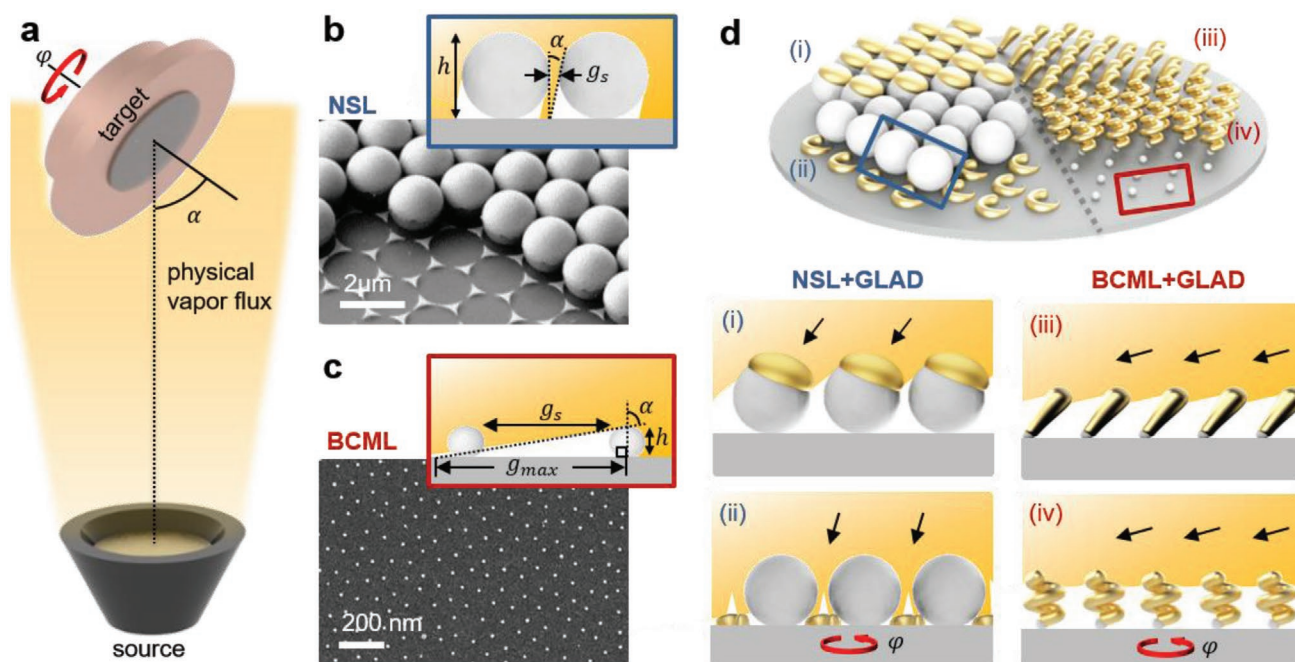


Figure 2. Glancing angle deposition (GLAD) on nanoseeds. a,b) Illustrations of physical shadow growth in a vacuum system (a), nanosphere lithography (NSL) with SEM image (b), and block-copolymer micelle nanolithography (BCML) with SEM image (c). a,b) Reproduced under the terms of the CC-BY Creative Commons Attribution 2.0 Generic license (<http://creativecommons.org/licenses/by/2.0>).^[108] Copyright 2013, The Authors, published by Beilstein-Institut. c) Reproduced with permission.^[25] Copyright 2013, Springer Nature. d) Combinatorial growth of 3D plasmonic nanostructures on NSL nanoseeds (i,ii) and BCML nanoseeds (iii,iv). (iii) and (iv) show the growth with substrate rotation.

target substrate during growth was proposed to change the direction of the incident vapor flux relative to the substrate, leading to the growth of nanostructured 3D films.^[102] This has been explored more systematically since the 1990s and is now often termed glancing angle deposition (GLAD).^[103] For simplicity, we here use “GLAD” for all types of physical growth techniques that entail shadowing (e.g., OAD without substrate rotation and GLAD with substrate rotation). GLAD has been used to grow helical and zigzag structures with dielectric materials,^[25] but it has been difficult to grow 3D-shaped metallic nanoparticles, a prerequisite for plasmonics.^[104] Due to the relatively high mobility of many metals, the adatoms experience a high surface diffusion such that they can move around during vacuum deposition to minimize their surface energy which hinders the fabrication of low-symmetry structures.

2.3. GLAD toward Nanoscale

Key factors to grow 3D metallic (or plasmonic) nanoparticles using GLAD therefore include a regular array of nanoscale seeds, such that all structures grow at the same rate. This is particularly important if the nanostructures should be uniform. In addition, the diffusion of adatoms needs to be suppressed. Here we summarize two approaches that can be used to address these challenges.

2.3.1. GLAD with Wafer-Level Nanoseeds

Deposition onto a bare wafer results in random nucleation sites and seeds that are not regularly spaced or of the same size. It follows that akin to Ostwald ripening the larger structures grow at a faster rate and hence the size distribution of the nanostructures broadens. This can be avoided if a regular pattern of seeds is presented onto which the vapor flux condenses. The smaller the structures of the seeds, the smaller the resulting nanostructures. Nanopatterns are, however, difficult to obtain on large areas.^[105]

A slow method that suffers from poor scalability is electron/ion-beam-based nanolithography. It can be used to obtain regular nanopatterns with customized shapes that can serve as nanoseeds, but is hardly a wafer-scale method.^[106,107] In contrast, techniques based on the self-assembly of spherical nanoparticles yield quasi-hexagonally close-packed seeds at the wafer-scale with very short processing times (e.g., <1 min for spin-coating). These work well in shadow deposition, including GLAD. Here, we focus on wafer-level GLAD schemes for the growth of plasmonic nanoparticles: nanosphere lithography (NSL, Figure 2b^[108]) and block-copolymer micelle nanolithography (BCML, Figure 2c^[25]).

The NSL is a capillary force driven method to closely assemble glass or polymer nanospheres (typically, from a few hundred nanometers to several micrometers in diameter) into a hexagonally close-packed lattice with spin- and dip-coating, or the Langmuir–Blodgett method.^[109] Refs. [40, 108, 109] present comprehensive reviews of GLAD in combination with NSL. The type of structure that is obtained when material is deposited onto the NSL seed layer depends on the angle of the

incident vapor flux. For $0 < \alpha < 90^\circ$, adatoms land on top of the closely packed nanoseeds (Figure 2d[i]). Depending on α , the surface coverage on top of the seeds can be varied from half coverage to a small cap on the seed particle, which, respectively, results in Janus structures^[43,110] and patchy particles.^[45,111,112] Similarly, metastructures including dimers are possible.^[113] The second approach uses a smaller α ($\lesssim 30^\circ$) to direct the vapor flux into the voids of the nanoseed particles, for example, the opening between three neighboring nanospheres in a hexagonal array. In this context, the nanoseeds are used as a flux-blocking mask where the opening forms an effective aperture giving rise to a seed gap, g_s with respect to α .^[114] Deposition through the aperture without azimuthal rotation ($\varphi = 0$) results in nanotriangles,^[115,116] while the continuous rotation during deposition leads to crescent (split-ring) and ring structures (Figure 2d[ii]).^[117,118] The gradual increase in the deposition rate while rotating the substrate during deposition further allows the growth of crescent nanoparticles that lack mirror symmetry and are thus chiral.^[52,119,120] As the structures are grown on top of the nanoseeds, the dimension of the resulting structures is in the range of several hundred nanometers to micrometers.^[40] A limitation, however, is that it is difficult to grow truly 3D-shaped plasmonic nanostructures.

In the previous example, the structural dimensions are approximately on the micrometer scale. In order to reduce the structural dimensions, nanoseeds much smaller than those found in NSL are necessary. For this the method of BCML can be used as it permits the fast, wafer-scale patterning of metallic nanoseeds (diameter 4–10 nm). The nanoparticle array serves as a seed layer for the subsequent GLAD step (Figure 2c).^[25,121,122] BCML is also a self-assembly technique, analogous to NSL. In BCML, block-copolymer micelles form in solution by self-assembly. Metal salts added to the solution accumulate in the core of the micelles. Upon spin coating onto a wafer, a quasi-hexagonal ordered monolayer of evenly spaced micelles is obtained. After plasma treatment, the block-copolymers are removed and the salts are reduced to form nanoparticles.^[25,123] The array of the nanoseeds can be ideally extended as large as the area of the target substrate to be coated, typically in the lab, silicon wafers with diameters of 2–4 inches are used. An array of 10 nm gold nanoparticles with 100 nm spacing are often used as a seed layer, but the center-to-center distance of the nanoparticles (max. ca. 300 nm) can be tuned by adjusting the polymer lengths, and the metal salt loading determines the diameter of the nanoparticles.^[121,124,125] In the GLAD step the maximal effective ballistic shadow distance between neighboring nanoseeds, g_{\max} obeys a simple geometrical relation,

$$g_{\max} = h \tan \alpha \quad (3)$$

where h is the seed height (diameter). For the seed dimension, $g_s > g_{\max}$, the evaporant strikes the substrate behind the shadowed region, and initiates the unseeded growth of nanostructures, potentially causing undesired additional plasmonic resonances.^[126] However, when the seed gap is reduced to $g_s < g_{\max}$, then columnar growth is observed without interstitial unseeded growth.^[100,127] The incident angle α in GLAD is generally very high ($>80^\circ$). A slow continuous rotation of

the substrate during growth leads to the formation of helically shaped chiral nanostructures (Figure 2d[iv]), while a fast or no rotation yields, respectively, vertical or slanted nanorods normal to the substrate (Figure 2d[iii]).^[127] Furthermore, when the size of the nanoparticle becomes larger (e.g., $h = 40$ nm), the shadowing region at the top and sidewall of the seeds are no longer connected and it then becomes possible to realize out-of-plane or in-plane dimers that are also plasmonic.^[105,126]

2.3.2. GLAD with Reduced Adatom Mobilities

Controlling the diffusion of the adatoms during growth is essential to enable the formation of complex 3D-shaped metallic nanoparticles. Any residual thermal energy of mobile adatoms leads to their diffusion and thus a collapse of any structural shapes (top panel of Figure 3a).^[25] To address this, it is possible to cool the substrate or to slow the diffusion by introducing dopants.

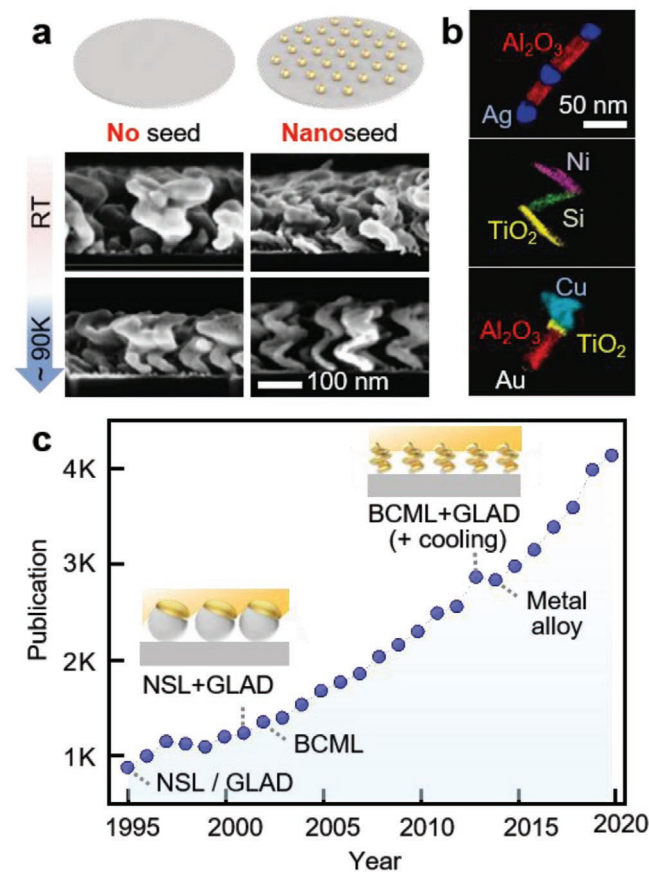


Figure 3. GLAD for the growth of 3D nanoparticles. a) Role of nanoseeds (right) and substrate cooling (bottom) during GLAD. b) False-color TEM images of 3D nanoparticles: barcode (top), zigzag (middle), and hook (bottom). a,b) Reproduced with permission.^[25] Copyright 2013, Springer Nature. c) Number of academic articles published each year containing the terms of physical shadow growth (or angle deposition, angle growth) with “plasmonic” since 1995. Source: Web of Science, as assessed on 27 July 2021.

According to the structure zone model^[128,129] where the film morphology is predicted according to the substrate’s temperature (T_s) and the melting temperature of source material (T_m) during growth (i.e., T_s/T_m), reducing the substrate’s temperature is effective to suppress the surface diffusion of adatoms. For instance, for metals the ratio should be $T_s/T_m < 0.24$ to achieve zone 1 conditions where structures grow in a columnar fashion.^[130] Hence, cooling the substrate (i.e., reducing T_s) by applying a coolant to the substrate holder, such as liquid nitrogen, during the deposition process can bring the substrate temperature to ~ 90 K and ensure columnar growth.^[25] As soon as the adatoms land, they then quickly lose their kinetic energy and freeze out at their present position. This enables the fabrication of very small structural 3D features using materials with mobile adatoms, such as metallic 2-turn nanohelices with a total height < 100 nm (bottom panel of Figure 3a) as well as barcodes, zigzags, and hooks with multiple material segments at the wafer scale (Figure 3b).^[25]

Another approach is to reduce the mobility not via cooling, but by introducing a dopant. Either an alloy or co-deposition is used and 3–5% (atomic percentage) of a secondary supporting material suffices to hinder adatom surface diffusion. The dopant should possess low thermal surface diffusion^[99] and a high melting point (T_m) to increase the net melting temperature (i.e., decrease T_s/T_m) such that zone 1 conditions can be reached while maintaining the substrate temperature. Through co-evaporation of the source material with the dopant together, Ag nanohelices with 3–5% Ti doping have been grown without noticeable change in their plasmonic property,^[54] and these structures enabled the observation of new nonlinear optical effects and spectroscopy from a single chiral nanostructure (see Section 5.3).^[60]

Interestingly, a further increase in the Ti doping level can be used to engineer the dispersion of a composite’s dielectric function. For instance, doping a plasmonic metal such as silver or gold with Ti flattens the dispersion curve (dielectric response as a function of wavelength) and consequently leads to a more sensitive plasmon resonance, because the resonance wavelength now changes by a greater amount for the same change in the dielectric function of the surrounding medium (e.g., Equation (4)). Shadow-grown hybrid plasmonic nanoparticles of this type have been used to observe greatly enhanced LSPR sensitivities that are much bigger than for undoped plasmonic nanostructures made of pure elements (see Section 4.2). Thanks in part to the development of wafer-level GLAD schemes, in particular seeding with NSL or BCML that offer a precise control over structure at the nanoscale in conjunction with substrate cooling in 2013^[25] and/or dopant-induced reduced mobility in 2014,^[99] the number of studies and publications in the field of GLAD for plasmonics rapidly increases every year (Figure 3c). An important aspect is 3D-shaped complex hybrid nanomaterials that are continuously being developed to unlock the full potential of plasmonics for diverse applications.

3. Complexity of Hybrid Nanomaterials

With an aim to gain an overview of the diverse hybrid plasmonic nanomaterials grown by GLAD, ranging from a symmetric

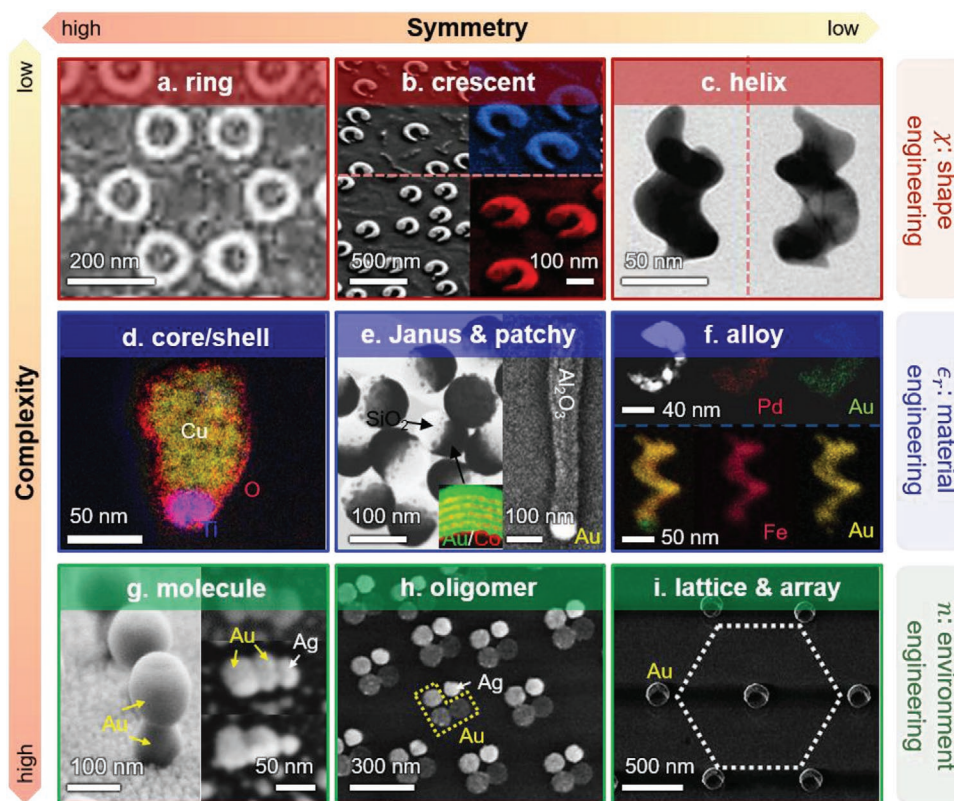


Figure 4. Classification framework of hybrid plasmonic nanostructures: a) rings, b) crescents, c) helix, d) core/shell particle, e) Janus and patchy particles, f) alloyed particles, g) metamolecules, h) meta-oligomers, i) lattice and array of particles (here, crescents). a) Image for rings: Reproduced with permission.^[118] Copyright 2009, Wiley-VCH. b) Image for crescents: Reproduced with permission.^[120] Copyright 2013, American Chemical Society. c) Image for helix: Reproduced with permission.^[25] Copyright 2013, Springer Nature. d) Image for core/shell particle: Reproduced under the terms of the CC-BY Creative Commons Attribution 4.0 International license (<https://creativecommons.org/licenses/by/4.0>).^[44] Copyright 2017, The Authors, published by Wiley-VCH. e) Image for Janus particles. Left: Adapted with permission.^[110] Copyright 2018, Wiley-VCH; Right: Adapted with permission.^[131] Copyright 2018, American Chemical Society. f) Images for alloyed particles. Bottom: Adapted with permission.^[53] Copyright 2016, American Chemical Society; Top: Adapted with permission.^[82] Copyright 2017, Wiley-VCH. g) Images for metamolecules: Reproduced with permission.^[126] Copyright 2019, American Chemical Society. h) Image for meta-oligomers: Reproduced with permission.^[132] Copyright 2014, American Chemical Society. i) Image for lattice and array of particles: Reproduced under the terms of the CC-BY Creative Commons Attribution 4.0 International license (<https://creativecommons.org/licenses/by/4.0>).^[133] Copyright 2020, The Authors, published by Wiley-VCH.

rod and ring structure to an asymmetric Janus, chiral crescent shapes, and helical nanoparticles, we propose to classify hybrid plasmonic nanomaterials according to their structure and symmetry, **Figure 4**. At the same time, we also consider the properties they exhibit and thus three main engineering spaces, namely: (i) χ , shape engineering, (ii) ϵ_r , material engineering, and (iii) n , engineering the environment (here, strictly speaking the arrangement or many nanostructures). This classification framework supports the comparison and design of hybrid plasmonic nanostructures in a systematic fashion and highlights which shape–material property relationship underlies a number of desired optical properties. It also aids the subsequent discussion. Although many other nanostructures previously fabricated are not listed in the framework due to space limitations, they can nevertheless be classified according to the same criteria. For example, the hybrid zigzag and hook structures in **Figure 3b** are of relatively low symmetry and contain several segments with different materials, and can therefore be positioned somewhere in between Janus nanoparticles (**Figure 4e**) and an alloyed chiral helix (**Figure 4f**).

3.1. Material and Shape Complexity

The y-axis (from top to bottom) of the classification framework (**Figure 4**) indicates the change in material complexity of hybrid plasmonic nanomaterials, which refers to the number of types of materials and segments within a given nanostructure and its arrangement. The left column shows structures with increasing complexity starting from pure Au nanorings (**Figure 4a**),^[118] Cu/HfO₂ core/shell nanorods (i.e., complexity increase in material, **Figure 4d**),^[44] to Au/Ag heterodimers or trimers arranged in-plane or out-of-plane (i.e., complexity increase in material composition and geometry/geometrical arrangement, **Figure 4g**).^[126] It is used to indicate three properties that are of interest for plasmonic applications: shape χ , dielectric function (material composition) ϵ_r , and interactions in lattices of plasmonic structures n , which are all of interest in engineering the LSPR response (see **Section 4** for details).

The core/shell nanoparticles consist of a plasmonic core encapsulated in a shell (**Figure 4d**) of, respectively, molecules,^[51,134] polymers,^[51,135–137] or inorganic materials.^[44,138] The

shell can increase the chemical and colloidal stability, ensure biocompatibility and prevent fouling.^[44] When the core consists of a nonmetallic material, for example, plastic^[45,110] or glass,^[139,140] it can be partially coated by GLAD to form plasmonic Janus or patchy nanoparticles (Figure 4e),^[110,131] or core-shell nanoparticles whose shell are plasmonically active and can even be formed from refractory materials, such as TiN.^[141] It is also possible to assemble superstructures with plasmonic building blocks, or “atoms,” to form metamolecules. These are distinct assemblies of nanoparticles (Figure 4g) to form dimers, trimers, tetramers, and oligomers (Figure 4h). All of the structures are grown by GLAD, including the one grown on BCML as helices (Figure 4c).^[25] GLAD with NSL at $\alpha < 30^\circ$ produces rings, crescent shapes (Figure 4b,^[120] also on a periodic lattice, Figure 4i),^[133] and oligomers.^[132,142] The Janus and patchy particles can be grown with varying degrees of surface coverage simply by changing α .

Apart from layered structures it is also possible to form alloyed hybrid plasmonic nanomaterials (Figure 4f^[53,82]). Since many materials can be deposited by PVD it becomes possible to realize a large combination of polyelemental nanoparticles with GLAD. For instance, by alloying a plasmonic metal (Au or Ag) with a second material (e.g., Pd, Ti, or MgF₂) the dielectric function can be changed and this can be exploited to achieve superior LSPR sensing.^[54,55,143] Similarly, additional functionalities can be introduced by combining the relevant materials, such as plasmonic and ferromagnetic,^[144–147] catalytic,^[81,148,149] and gas responsive active plasmonic nanoparticles^[150,151] (see Section 4.2 for details).

3.2. Symmetry and Chirality

The x -axis (from left to right) in the classification shows a reduction in the symmetry of the individual nanoparticle (Figure 4). Using the point group symmetry, nanorings, core/shell nanorods, and linear dimers on the left show higher symmetry ($D_{\infty h}$) than Janus nanoparticles and hetero trimers ($C_{\infty v}$), and low-symmetry chiral tapered nanoparticles (C_1) and hetero oligomers (C_2). Chiral nanoparticles can be grown by GLAD, for example, with BCML for nanohelices with a slow azimuthal substrate rotation,^[25] as well as with NSL for nanocrescent structures between seed particles^[52] or as multilayered patchy particles on the top of seeds.^[152,153]

Aside from the symmetry of the nanoparticle's geometry, the symmetry of the nanoparticles' arrangement is particularly important, when the lattice constant approaches the wavelength of the LSPR band (Figure 4i).^[133] A new lattice resonance mode can be observed that couples to the LSPR, thanks to the additional diffraction of the scattered light through the lattice (see Section 4.3 for details).^[154] The symmetry of the hexagonal lattice in NSL and BCML can be tuned by, respectively, controlling the sizes of spheres and micelles (to be assembled).

4. LSPR Engineering

The LSPR is determined by the nanoparticle's shape χ , material ϵ_r , and the surrounding environment n (Equation (2) and

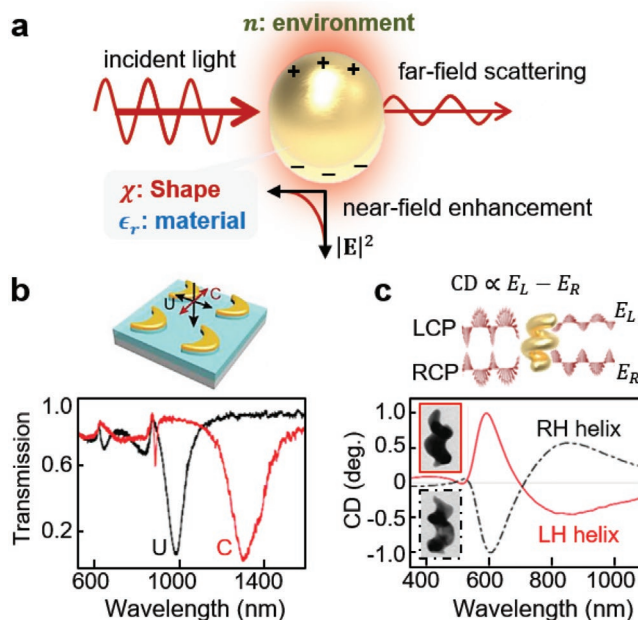


Figure 5. LSPR of shape-engineered plasmonic nanoparticles. a) LSPR phenomena of a metal nanosphere under light illumination. b) Linear-polarization dependent LSPR signals of nanocrescents. U and C, respectively, indicate the light polarization along the short and long axes of crescents. Reproduced with permission.^[61] Copyright 2019, Wiley-VCH. c) Circular dichroism (extinction) spectroscopy of nanohelices (LH: left-handed, RH: right-handed). Reproduced with permission.^[25] Copyright 2013, Springer Nature.

Figure 5a). Here, “LSPR engineering” refers to the systematic design and control of those factors that determine the form and spectral position of the LSPR and its associated functions, such as the generation of hot electrons,^[155–157] heat,^[5,9,11,131,158] and acoustic waves.^[159–161] These are included in the classification (from top to bottom, Figure 4). The first two groups, shape and material engineering, focus on the LSPR of individual nanoparticles, whereas the last group, environment engineering, concerns the near- and far-field coupling of nanoparticle arrangements, which influence the “effective” refractive index n of the surrounding. We highlight the role of the engineering space in the emerging field of nanophotonic material and device applications.

4.1. Shape Engineering

The resonance wavelength of a nanostructure depends on shape. Shadow growth can be used to obtain isotropic spheres (typically, in the range of 10–100 nm) as well as anisotropic and/or low symmetric structures (e.g., the first row in Figure 4). The relevant length scale in plasmonics only applies to the overall size of the plasmonic material in the nanoparticle. For instance, the Janus pen consists of a small plasmonic nanoparticle (ca. 80 nm in diameter) at the end of the 500 nm long oxide rod (Figure 4e).

An increase in length or shape complexity of the plasmonic section along one or more axes of the nanoparticle introduces the appearance of additional LSPR modes, such

as a longitudinal mode (LSPR along the long axis). It is red shifted with respect to that of the transverse mode (LSPR along the short axis), Figure 5b.^[61] Since the anisotropic geometry increases the polarizability along the long axis of the plasmonic nanoparticle, this causes the additional extinction band in the NIR, which can be modulated by controlling the geometrical anisotropy, specifically the aspect ratio of the rods^[162] and crescents.^[52] A strong extinction feature in the NIR benefits in in vivo biomedical applications owing to the NIR transparent window of human tissue,^[163,164] such that the plasmonic nanoparticle can for example be used as a sensing probe^[164] and as a contrast agent in photothermal imaging,^[11,165,166] or a carrier for drug delivery^[167,168] (see Section 5 for applications).

An attractive feature of GLAD is that it can be used to grow chiral nanoparticles with uniform shape and definite handedness. Chiral nanoparticles possess identical physical and chemical properties, but can be distinguished in a chiral interaction.^[169] For instance, they interact differently with left- and right-circularly polarized light (e.g., bottom panel of Figure 1b), which is termed optical activity.^[170] The differences in the real part (refractive index) and imaginary part (extinction) of the complex refractive index with respect to left- and right-polarized light, respectively, underlies circular birefringence (CB) and circular dichroism (CD). Among several methods that probe the chirality,^[171] CD spectroscopy (strictly circular extinction) is suitable for the study of both colloidal forms and nanostructured substrates of plasmonic nanoparticles (Figure 5c). Because the LSPR can be tuned, it is also possible to move the chiral band to longer wavelengths outside the absorption range of regular biological media, such as blood.^[53] The optical activity of chiral nanostructures is also much stronger than that associated with molecules, so that it becomes possible to observe the chiral response of a single chiral nanoparticle^[59] as well as nonlinear optical signals from suspensions^[60,172] (see Section 5.3 for details). The chiroptical effect can be tailored by engineering their geometry (e.g., helix: pitch, major, and minor radius,^[54] oligomer: height and gap^[173]) as well as material composition.

4.2. Material Engineering

The purpose of incorporating other materials and/or segments in a plasmonic nanoparticle (the second row of the classification in Figure 4) is to address dispersion engineering for customized coloration and superior sensing performance.^[54,174] It also serves to introduce multiple functions within a single nanostructure.^[23,144–151,175,176] Materials for LSPR typically include metals, such as Au,^[25,52,59,120,126,132,162,177–182] Ag,^[60,134,182–191] Cu,^[123,192] Ni,^[192,193] Pd,^[82] Mg,^[192,194] and Al^[192,195] whose LSPR bands are intrinsically set by their plasma frequencies (Figure 6). They are the key component in the LSPR response, which can be further modified by alloying them with other plasmonic or functional materials (i.e., increase in the material complexity from top to bottom in the framework in Figure 4). For instance, the gradual change in the atomic ratio of Ag and Cu through the whole body of a single nanotriangle modulates the peak position of LSPR spectra over a wider spectral band than is possible with either material alone (Figure 6b,c). This is because the effective dielectric constant of the alloyed material changes. In particular, by alloying a plasmonic material with a weakly dispersive one, it becomes possible to obtain a flatter ϵ_r curve while ensuring ϵ_r is still negative (e.g., see Figure 7a).^[54] Examples are Ag helices doped with Ti (3–23%)^[54] and Ag patchy particles doped with MgF₂ (3–10%)^[55] giving rise to the extended LSPR bands, respectively, ranging from 347–920 and 890–1537 nm (Figure 6c).

Apart from the role of tunable coloration, dispersion engineering also offers a route to increase the sensitivity in LSPR detection.^[54] LSPR sensing relies on detecting a change in the local refractive index n^* surrounding a plasmonic nanoparticle via a change in the LSPR peak position λ^* (Equation (2)).^[54] and has been adopted for various chemical and biological sensors. Applications include the detection of food poisons,^[196,197] hazardous heavy metal ions,^[198,199] cancerous cells,^[165,200] and viruses.^[201] The crucial value to evaluate the sensing performance is the figure of merit (FOM = sensitivity/full width at half maximum [FWHM] of the resonance), where the LSPR sensitivity is given by^[69]

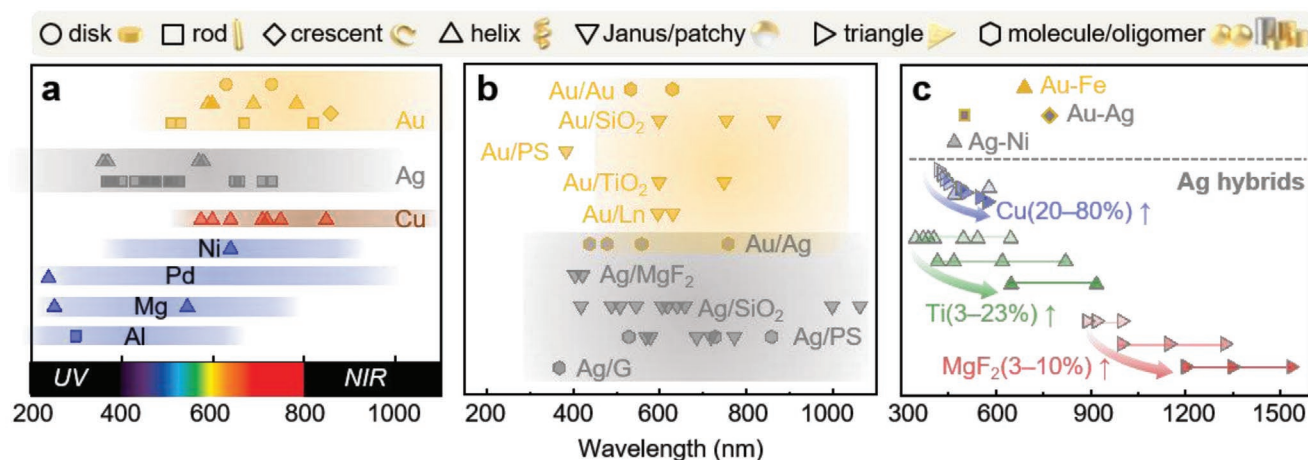


Figure 6. LSPR of shape- and material-engineered plasmonic nanoparticles. a–c) LSPR spectral bands of plasmonic nanoparticles made of: a) homogeneous metals (Au,^[25,52,59,120,126,132,162,177–182] Ag,^[60,134,182–191] Cu,^[123,192] Ni,^[192,193] Pd,^[82] Mg,^[192,194] and Al^[192,195]), b) multilayered shapes (Janus and patchy: Au/SiO₂,^[133] Au/polystyrene,^[208] Au/TiO₂,^[151] Au/Ln,^[62] Ag/MgF₂,^[209] Ag/SiO₂,^[139,210,211] Ag/PS,^[152,153,212–214] and molecular structures: Au/Au dimer,^[126] Au/Ag dimer and trimer,^[126,132] Ag/G dimer^[215]), and c) metal alloys (Au–Fe,^[53] Au–Ag,^[216] Ag–Ni,^[123] Ag–Cu,^[25,56,123,217] Ag–Ti,^[54] and Ag–MgF₂^[55]).

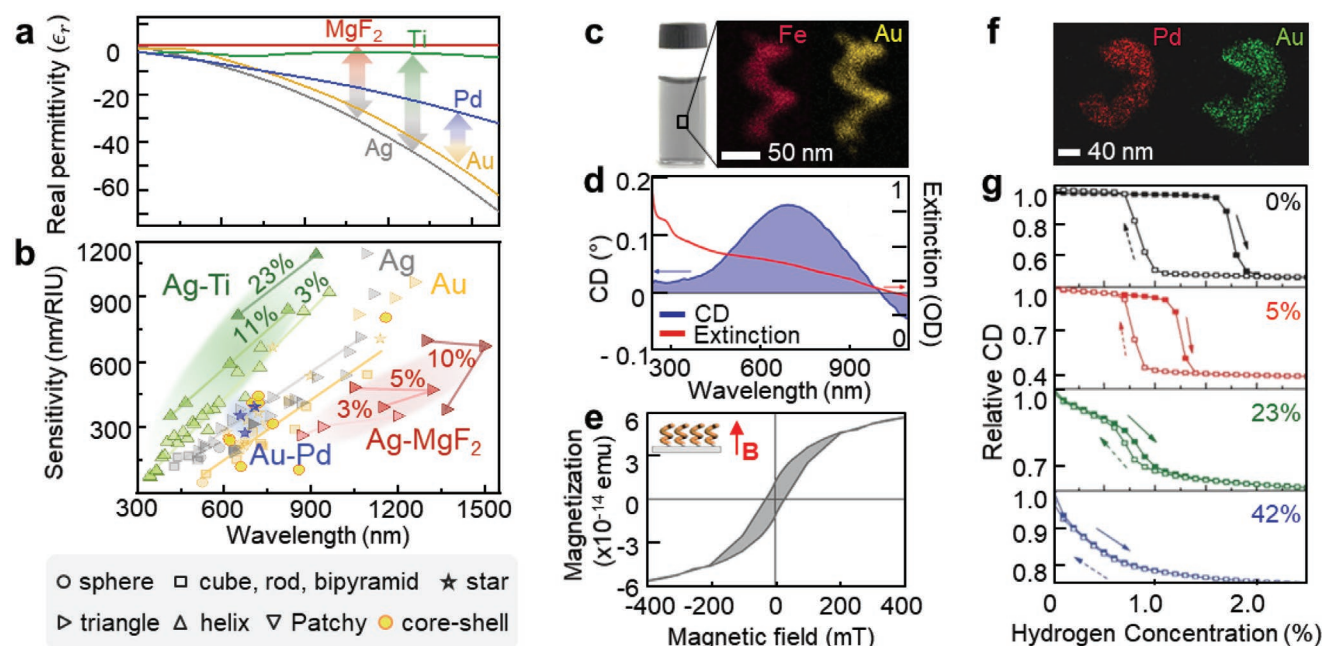


Figure 7. Multifunctional alloyed plasmonic nanoparticles. a) Dispersion of the dielectric constant (ϵ_r) for Au,^[224] Ag,^[224] Pd,^[225] Ti,^[225] and MgF₂.^[226] b) Reported LSPR sensitivities of nanoparticles (sphere,^[203,205,227,228] triangle,^[55,204,227,229,230] star,^[143,203,231–234] cube,^[203,235–237] rod,^[202,203] bipyramid,^[203] core-shell,^[234,238–242] patchy,^[243] and helix^[54]). c–e) Au–Fe nanohelices and c) a colloidal suspension and TEM image thereof, d) LSPR (red: extinction, blue: CD), and e) magnetic properties. c–e) Reproduced with permission.^[53] Copyright 2016, American Chemical Society. f,g) Au–Pd nanohelices' TEM image (f) and CD changes (g) as a function of hydrogen concentration. f,g) Reproduced with permission.^[82] Copyright 2017, Wiley-VCH.

$$S_n = \frac{d\lambda^*}{dn^*} = \frac{\frac{d\epsilon_r^*}{dn^*}}{\left(\frac{d\epsilon_r}{d\lambda}\right)_{\lambda^*}} = \frac{-2\chi n^*}{\left(\frac{d\epsilon_r}{d\lambda}\right)_{\lambda^*}} \quad (4)$$

The traditional way to improve the sensitivity (eventually FOM) is via shape engineering (χ), for instance by employing anisotropic particles (e.g., rods^[202,203] and prisms^[204]). This, however, yields sensitivities that are typically below 1000 nm per RIU (refractive index unit, Figure 7b),^[205] which is still one to two orders of magnitude lower than those of surface plasmon resonance biosensors.^[206] A recently developed alternative approach is to decrease the wavelength dependence of ϵ_r (i.e., dispersion engineering to reduce the denominator in Equation (4), Figure 7a), leading to further increase in sensitivity (Figure 7b). Examples are (but not limited to) Au–Pd,^[82] Ag–MgF₂,^[55] and Ag–Ti,^[54] allowing enhanced sensitivity compared to the same structure made from a pure metal. The latter, in particular, holds the record sensitivity over 1000 nm/RIU while keeping the resonance in the visible range.^[54] It is of interest to further explore the optimal material alloy composition to reduce absorption effects (i.e., large FWHM) and in this context high-dielectric materials are of particular interest.^[207]

An interesting development is the combination of a nanostructure that shows LSPR with another property, such as a magnetic,^[144–147,218] catalytic,^[148,149] or gas responsive material.^[150,151] For this purpose hybrid nanoparticles can be fabricated by GLAD, as shown in the second row of the framework in Figure 4. Examples include magneto-plasmonic

core/shell particles (Au/Fe₂O₃^[219] and Fe₂O₃/Au^[220]), Janus (Au/Co multilayered patchy on polymeric particle, left panel of Figure 4e),^[110] and Au–Fe alloyed chiral nanohelices (bottom panel of Figures 4f and 7c).^[53] Since both plasmonic (Figure 7d) and magnetic functions (Figure 7e) are still active in the hybrid nanoparticles, an external magnetic field can be used to align the particles in solution and thereby modulate the LSPR. Similarly, “active” plasmonic systems can be actuated for optical signal modulation.^[47]

Another example is hydrogen sensing with Au/Pd multilayered structures^[221] or alloyed nanostructures^[82] (Au–Pd helix in Figure 7f). When exposed to hydrogen, the Pd undergoes a reversible phase transition from the metallic state to a hydride and thus changes its dielectric constant (and hence the LSPR signal), making Pd suitable for hydrogen sensing.^[222,223] A drawback is that the LSPR signal is broad and featureless,^[82] and shows hysteresis in gas adsorption/desorption with long response times (e.g., 40 min for ca. 2% hydrogen sensing). Much sharper and stronger LSPR signals are observed when Au is alloyed with Pd (Figure 7g). Crucially both the hysteresis and response time are also significantly reduced, which makes the Pd–Au hybrid chiral nanostructures useful for plasmonic hydrogen sensing.^[82]

Hybrid plasmonic nanoparticles with responsive polymers are responsive to mechanical,^[137] optical,^[137,244] and electric inputs.^[47,245–248] Recently, the latter is extensively developed as a form of core/shell nanoparticle whose core is plasmonic and shell is a conductive polymer, for example, polyaniline. A promising application is the use of these hybrid nanoparticles as nanopixels for reflective displays^[249–251] and meta-atoms for active optical holography.^[137,248,252] The common underlying

mechanism here is that the change in the redox state of the conductive polymer in response to an applied voltage causes the change in its complex refractive index, n^* , leading to a shift in the LSPR peak, λ^* (i.e., color, referring to Equation (4) for LSPR sensing).^[77,136] To the best of our knowledge, the GLAD-grown nanoparticles have not been applied in this scheme, but the plasmonic hybrid nanomaterials could be promising as they can further increase the performance via dispersion engineering.

4.3. Environment Engineering

Here, we refer to environment engineering to describe the near- and far-field coupling between plasmonic nanoparticles (the third row of the classification framework in Figure 4). At short range (i.e., interparticle spacing $\lesssim 0.1$ particle size),^[253] the LSPs of neighboring nanoparticles are coupled and generate strong optical near-field enhancement, known as hotspots. These give rise to a new LSPR cavity mode (e.g., Figure 4h).^[254,255] The hotspot can be maximized by reducing the gap down to ca. 1 nm between plasmonic metamolecules (Figure 4g,h) and very often finds application in surface enhanced Raman scattering. The Raman signal is enhanced by many order of magnitude (depending on mechanism and analysis enhancement factors between 10^4 and 10^8 are quoted).^[256] Depending on shape and/or material composition (Figure 4h), the near-field coupling can also become polarization-dependent, which could be of interest in chiral sensing applications.^[132,257]

For larger separations between plasmonic nanostructures, collective LSPR effects can take place via the far-field coupling of diffracted scattering of neighboring nanoparticles within their lattice (Figure 4i).^[133,258] Interestingly, this effect can even occur for a sparse nanoparticle distribution, which approximates to the dimension of the LSPR peak position λ^* , and results in a strong and sharp resonance upon the LSPR signal, commonly referred to as plasmonic surface lattice resonance, SLR.^[154,259,260] The sharp (high Q-factor) resonance can be achieved when individual plasmonic nanoparticles are identical (i.e., same geometry and material composition) and arranged with a regular distance near λ^* .^[261] It has been utilized for selective light filtering,^[262] LSPR sensing to reduce the FWHM (so high FOM),^[263,264] and recently, the photonic lasing effect.^[61,265,266] Furthermore, this SLR still occurs under a chiral influence so gives rise to unique chiroptical lattice resonance, if the nanoparticles are chiral, for example, crescents (Figure 4i).

5. Emerging Applications

Engineering hybrid plasmonic nanomaterials controls the LSPR while incorporating additional functionalities. The following subsections highlight three recent key applications of hybrid plasmonic nanomaterials, namely in photonic devices (Section 5.1), biomedical applications (Section 5.2), and chiroptical spectroscopy (Section 5.3). The reader may consult refs. [1, 11, 267–269] for other possible applications using plasmonics.

5.1. Nanophotonic Devices

Over the last few decades, several new nanophotonic devices based on the LSPR have been developed including various types of optical modulators, for example, filters,^[270,271] diffrusers,^[244,272,273] polarizers,^[274,275] and wavelength (down or up) converters,^[62,276,277] as well as components of optoelectronic devices including lasers,^[61,276,278–280] light-emitting diodes,^[281–284] photodetectors,^[285–288] and photovoltaics.^[289–291] The advance in nanofabrication including GLAD helps to not only improve their performance, but also diversify the application domains ranging from high-end electronics to consumer products.^[283,284,292] Although there are many types of devices involved in this context, they share several underlying physical mechanisms. So, we here discuss them based on recent representative LSPR-based photonic applications, namely optical modulation (polarization, Figure 8a and energy, Figure 8b), conversion to electrons (photodetection, Figure 8c,d), and amplification (lasing, Figure 8e). The interested reader is referred to refs. [1, 4, 78, 157, 293, 294] for further information on photoelectric conversion and LSPR-based photonic devices.

The optical modulation using plasmonics is often based on the shape complexity of the plasmonic nanomaterials (as seen in the first row of the framework in Figure 4), where the optical extinction at the LSPR depends on the wavelength and polarization state of the incident light. For instance, the longitudinal LSPR mode is excited if the light polarization is parallel to the structural long axis of plasmonic nanorods, whereas negligible interaction occurs when the polarization is orthogonal.^[295,296] This simple mechanism applies to most LSPR-based optical modulators, as seen in an example of Au gratings on a wrinkled polymer substrate (Figure 8a).^[244] The simple GLAD process (with control of the vapor flux angle) onto the wrinkled polymer yields centimeter-scale Au nanogratings with the tunability of the spatial distance (left panel of Figure 8a). Arising from the dissimilar excitation of plasmonic modes due to the anisotropy, the intensity and angle of light diffracted into different diffraction orders differ (right panel of Figure 8a). The same modulation approach can be used for polarization-dependent coloration. For example, the forest of slanted Ge nanorods on a Au mirror can modulate colors across the whole visible range in response to the linear polarization of the incident light,^[275] which is potentially useful for holographic data encryption.^[252,297–299] and display applications.^[297,300–302]

An increase in the material complexity of plasmonic materials (as seen in the second row of the framework in Figure 4) can enhance the performance of the optical modulator. For example, plasmonic patches on lanthanide nanoparticles lead to the superior efficiency of photon upconversion (i.e., the color conversion from NIR to visible) compared to those supported by the lanthanide nanoparticle alone (Figure 8b). Lanthanide nanoparticles covered with Au can show plasmonic hotspots at openings on the surface, and it is from there that photons are concentrated, resulting in the enhanced photon upconversion and extraction, while the details are still unclear since multiple routes of upconversion can occur at the same time.^[62]

Such plasmonic hotspots in the extremely small gap between plasmonic elements, that is, metamolecules (as seen in the third row of the framework in Figure 4), can also be used

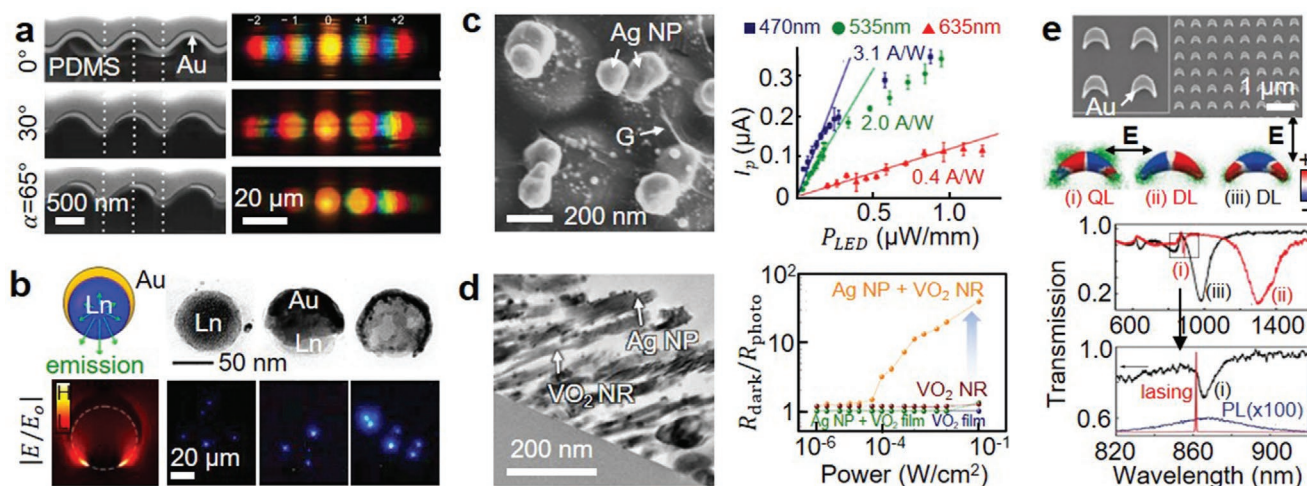


Figure 8. LSPR photonic devices. a) Au gratings on PDMS (SEM, left) and associated diffraction patterns under constant light illumination (right). Reproduced under the terms of the CC-BY Creative Commons Attribution 4.0 International license (<https://creativecommons.org/licenses/by/4.0/>).^[244] Copyright 2021, The Authors, published by Wiley-VCH. b) Au/lanthanide Janus nanoparticles with different Au surface coverages (TEM, top) and associated theoretical optical field enhancement and experimental upconverted light generation (bottom). Reproduced with permission.^[62] Copyright 2017, American Chemical Society. c) Ag dimers with a graphene sandwich structure between them (SEM, left) and their associated photocurrent generation in response to red (635 nm), green (535 nm), and blue (470 nm) light wavelength at 180 K. Reproduced with permission.^[113] Copyright 2015, Wiley-VCH. d) Ag-decorated VO₂ nanorods (TEM, left) and associated photoresistance. Reproduced with permission.^[83] Copyright 2019, American Chemical Society. e) Array of Au nanocrescents (SEM, top) and associated changes in charge distributions, LSPR spectra, and lasing emission spectra according to direction of the linearly polarized light (middle and bottom). Reproduced with permission.^[61] Copyright 2019, Wiley-VCH.

for photoelectric conversion (Figure 8c).^[113,303] The array of standing Ag nanodimers with a graphene spacer (ca. 0.34 nm) was fabricated by GLAD (left panel of Figure 8c) and used for a 100-fold optical field enhancement,^[113] leading to the plasmonically enhanced photoresponse as high as 14.5 A W⁻¹ at $\lambda = 280$ nm, which corresponds to a 10 000-fold enhancement over the photoresponse of native graphene.^[215] The LSPR feature of Ag plasmonic nanoparticles can be also combined with phase change materials, for example, VO₂ for enhanced photoelectric conversion (Figure 8d). When the simulated solar spectrum (AM 1.5G) is illuminated, the near-field enhancement of the Ag nanoparticles leads to a change in the phase of VO₂ from dielectric to the metallic state, resulting in a ten-fold increase in conductivity.^[83] A similar mechanism can also be observed with responsive polymers.^[47,78,137] For example, plasmonic nanostructures are encapsulated within conductive polymers (e.g., polyaniline,^[77,136,247] poly(3,4-ethylene-dioxythiophene),^[245,247,248] polypyrrole,^[246,247,304] and poly(3,4-(2,2-dimethylpropylenedioxy)thiophene)^[305]), acting as electrochromic elements for future low power-driven reflective displays^[249–251] and active holographic displays.^[35]

In contrast, sparsely arranged plasmonic nanostructures can generate far-field optical coupling and enhancement (Figure 8e),^[61] which could be another route to make active plasmonics for photonic applications.^[47,133,136,265] For instance, an array of nanocrescents gives rise to a polarization-dependent plasmonic lattice resonance, that is, the long axis of the crescents supports an additional higher mode, that is, quadrupolar lattice mode, due to the broken symmetry in the structure.^[306] The lattice resonance stems from the in-plane component of the scattered light supported by individual plasmonic nanoparticles, which can be diffracted and trapped if the lattice dimension of the nanoparticles matches the wavelength of the

scattered light.^[133,154] The trapped state of the light (in accordance with the quadrupolar lattice mode, not the dipole lattice mode, middle panel of Figure 8e) means efficient accumulation of photons in the lattice and thus makes it possible to induce photon emission stimulated by injecting trigger photons, that is, lasing (bottom panel of Figure 8e). This nano-lasing mode is not only switchable by changing the polarization of an external light field,^[61] but can also be used to tune the color by controlling the surrounding refractive index or lattice parameter.^[133,265,266,307–309] We expect that such lasing effects can be further engineered by increasing the complexity, for example, metal alloys for enhanced scattering or incorporating additional functionalities and/or reducing the symmetry (e.g., more anisotropic or chiral) and that they find many potential applications, including in sensing and active displays.^[251,310,311] Recent advances in hybrid plasmonic systems and their large-scale fabrication, often utilizing shadow growth methods, accelerate the translation of current research activities into the industrial domain for real-world applications.

5.2. Biomedical Applications

LSPR systems are valued for their strong optical response and small size so they are important for various biomedical applications, ranging from in situ disease detection and diagnosis^[312–314] to noninvasive local surgery and treatment,^[158,165,168,315] and recently actuation inside the human body aiming for nanorobotics.^[53,63,316] Hybrid plasmonic nanomaterials grown by GLAD permit the combination of two or more functions within a single nano-object, which is needed in nanorobotic applications.^[205,317] Due to the broad range of possible biomedical applications, we here focus on examples

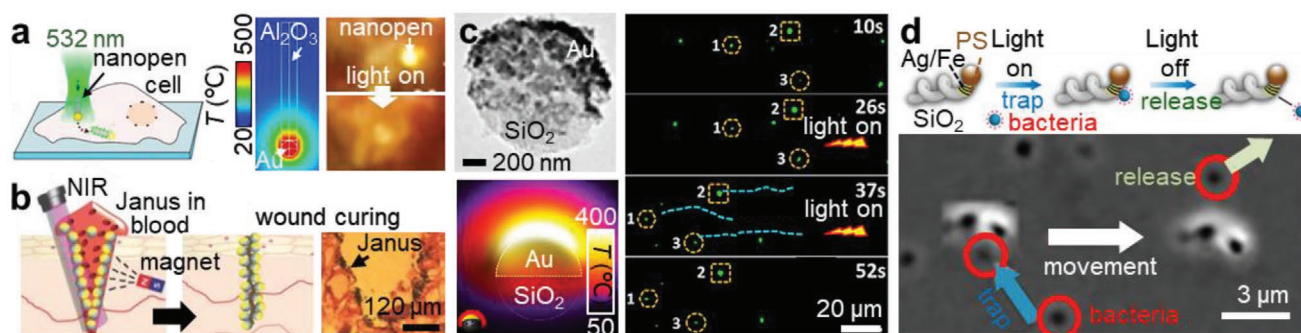


Figure 9. Hybrid plasmonic nanomaterials for biomedical applications. a) Au/Al₂O₃ Janus nanopen for the intracellular penetration via the photo-thermal effect (left) and experimental observation of the nanopen penetration (right). Reproduced with permission.^[131] Copyright 2018, American Chemical Society. b) Au/Fe₃O₄ magneto-plasmonic Janus nanospheres for tissue fusion (left) and the experimental observation (right). Reproduced under the terms of the CC-BY Creative Commons Attribution 4.0 International license (<https://creativecommons.org/licenses/by/4.0>).^[64] Copyright 2016, The Authors, published by Wiley-VCH. c) Au/SiO₂ Janus nanoparticle and its simulated photothermal effect (left), and experimental motion in water (right). Reproduced with permission.^[76] Copyright 2016, American Chemical Society. d) SiO₂ micro helix with Ag/Fe patchy at one end for magnetic propulsion with plasmonic trapping (top) and corresponding experimental demonstration for active cargo delivery (bottom). Reproduced with permission.^[63] Copyright 2018, The Authors, published by American Association for the Advancement of Science.

that benefit from GLAD-grown hybrid plasmonic nanomaterials. The first is the photothermal effect for cell penetration (Figure 9a) and fusion (Figure 9b) as well as the actuation of the nanoparticle (Figure 9c). The next is the optical force to be used as a tweezer for active cargo delivery with self-propelling micro actuators (Figure 9d). We refer the reader to refs. [205, 316, 318] for more comprehensive general reviews on the plasmonics for biomedical applications including sensing, imaging, drug delivery, and hyperthermia.

Excitation of a metallic nanoparticle at the LSPR generates heat via the Joule effect, known as plasmonic heating, and the increase in the temperature is proportional to the light absorption.^[163] The Janus-type plasmonic nanopen composed of a Au nanosphere connected to a dielectric (Al₂O₃) handle (Figure 9a) generates heat only at the plasmonic tip, enabling the entire nanopen to drill through the cell membrane of a living cell while maintaining a cell viability of over 75% (right panel of Figure 9a).^[131] The handle-like body can be chemically functionalized with DNA. Injection of the nanopen into a cell with an optical tweezer, then permits DNA to be directly inside a living cell, as the handle stays cold. The plasmonically heated nanotip opens a pore in the membrane and thus permits the spatially controlled injection of genetic material with an untethered nanocarrier, which is potentially useful for future applications in cell transfection or sensing.^[163,316] Different hybrid magneto-plasmonic Janus particles have been used as a glue to suture wounds in a living mouse (Figure 9b).^[64] An external magnetic field drags and localizes the Janus particles near the area of the physical wound, and heat is generated by the NIR light exciting the LSPR of the plasmonic particle. In vivo applications can be envisioned due to the long penetration depth through skin and tissue of NIR light. Plasmonic heating initially causes blood aggregation near the Janus particle, resulting in blood coagulation to prevent excessive bleeding, and further aids the synthesis of collagen, ultimately accelerating the healing process. The long-term stability of the nanoparticles (i.e., toxicity and biodegradability) still needs to be addressed.

It is also possible to realize self-propelling microparticles with hybrid plasmonic structures. The LSPR-driven photothermal

mechanism can be combined with plasmonic nanoparticles that are anisotropic or that possess low symmetry, such that light absorption generates a nonuniform thermal profile around the particle. The temperature gradient across the particle induces fluid flows and the particle moves. Termed self-thermophoresis, the particles' motion now has an additional active ballistic component in addition to its Brownian motion.^[319] For example, a Janus nanoparticle whose core is a glass (SiO₂) sphere coated with a Au cap at one hemisphere can generate thermal gradient surrounding the nanoparticle under NIR light irradiation matching to the LSPR peak (left panel of Figure 9c), leading to the propulsion of the nanoparticle with the maximal velocity of $\approx 18 \mu\text{m s}^{-1}$ in water (right panel of Figure 9c).^[76] If the SiO₂ core is mesoporous, it can simultaneously act as a cage to carry drug molecules such as doxorubicin, gemcitabine,^[320] and cisplatin.^[321] Another intriguing example of LSPR for actuation is optical force-driven actuation,^[322] which could benefit from GLAD-grown nanomaterials.^[322–325] For example, a pair of asymmetric Au nanorods with different lengths (130 and 175 nm) on a substrate generates strong optical near-field coupling and induces directional scattering which can push the entire object forward.^[324]

One advantage of helical or rod-shaped tiny nanomachines is that in complex biological fluids, which is often a non-Newtonian viscoelastic environment,^[326] propulsion experiences less hindrance if the cross section is smaller than the mesh size of the macromolecular network of the medium.^[327] The nanoparticles can then move in the fluid in the pores, which at this small scale then behaves as a simple Newtonian fluid.^[53,326,328] Various types of forces, including optical,^[329,330] magnetic,^[331–333] acoustic,^[334–337] catalytic,^[338–341] and thermal forces^[11,342–344] are used to drive the motion of the nanoparticles. Among them, the most advanced scheme with the prospect for biomedical applications is a magnetic force driven actuation of micro/nanohelices. The body of the helix can be made from a variety of materials including oxides (SiO₂) and one section typically contains a ferromagnetic material for magnetic actuation (top panel of Figure 9d). The magnetic moment should be orthogonal to the long axis of the helix, such that an

externally applied rotating magnetic field can rotate the helix, which then translates due to rotation–translation coupling.^[53,63] These micro/nano helices can be functionalized to propel in mucus,^[345] living cells,^[346] and pig eyes.^[147] Most recently, it has been shown that a biocompatible magnetic material that at the same time is a hard ferromagnet with a record magnetization, namely FePt in the L1₀ phase, can also be incorporated in hybrid nanostructures via GLAD.^[51]

The nanomachines can also be decorated with plasmonic nanoparticles to optically trap and release a payload (Figure 9d).^[63] The alternately deposited Fe and Ag structures at the neck part of the helix are used for magnetic propulsion and at the same time give rise to optical near-fields that exert an optical force on bacteria and liposomes when illuminated. The goal of actively propelling hybrid structures is targeted delivery, which has many potential benefits over traditional systemic passive diffusion-based drug delivery in the body.^[347]

5.3. Chiroptical Spectroscopy and Chiral Sensing

Chirality plays an important role in biology and chemistry, and most newly approved pharmaceutically active compounds are chiral (handed). The foremost technique to distinguish the two mirror-image forms of a chiral molecule is optical. Chiroptical spectroscopy relies on the differential interaction of chiral (handed molecules) with handed or left- and right-circularly polarized light. A difference in the absorption of left- and right-circularly polarized light is known as CD,^[257] which can also be detected as fluorescence-detected CD,^[348] or when the resonances are vibrational as vibrational CD.^[349] Corresponding differences in the real part of the refractive index are observed as optical rotation, and its variation with wavelength as optical rotatory dispersion,^[171] and for vibrational resonances as Raman optical activity.^[350] All of these optical effects rely on a change of the light's electric (and magnetic) field across the molecule. Hence, these effects are small as the wavelength of light is many orders of magnitude larger than a molecular dimension.^[171] Nanostructures that are chiral therefore show much larger effects. In addition, plasmonic chiral nanostructures benefit from stronger light–matter interactions at the plasmon resonance frequency. Both effects greatly amplify the chiroptical response.^[351–356] The reader may want to consult^[37,169,171,257,357,358] for comprehensive reviews of chiral plasmonics and spectroscopy, also for an ongoing discussion on the underlying physical mechanisms.^[359]

Plasmonic nanostructures show strong scattering effects, which permits the observation of a single nanoparticle using a dark-field spectroscopy.^[59,360,361] Analyzing the difference of the scattering response to circularly polarized light underlies single particle chiroptics. The corresponding circular differential scattering intensity (CDSI), defined as^[362]

$$\text{CDSI} = \frac{I_L - I_R}{I_L + I_R} \quad (5)$$

where I_L and I_R are the intensities of scattering from the nanoparticle in response to, respectively, left- and right-circularly polarized light (Figure 10a). The spectra from a single chiral

plasmonic nanoparticles including oligomers^[173] and helioids^[363] are successfully observed using this method. One difficulty is that often the nanostructures are positioned on a substrate, which complicates the interpretation, as the sensitivity to circularly polarized light may not only stem from the particles' intrinsic chirality, but also from the particle's orientation on the substrate.^[37,364,365]

Shadow-grown chiral GLAD structures, including crescents,^[118] hooks,^[25] and helices (shift from left to right in the framework in Figure 4),^[59,193,366] can also be used in suspension.^[44,53,54,60,172] A colloidal suspension of plasmonic nanohelices can serve as a reference sample to ensure a setup that measures the intrinsic chirality of the structures and not a geometrical artefact.^[59] In dilute suspensions (typically, pico-molar concentration) where the interparticle separations are large, the chiral nanoparticles independently undergo Brownian motion and thus maintain random orientations in space.^[59] The chiral plasmonic response in such an isotropic state is given by the average response across all possible nanoparticle orientations, that is, the ensemble-averaged CDSI (bottom panel of Figure 10b).^[59] Interestingly, a single particle in solution will over time also sample all orientations in space. Hence, the time average of the CDSI of a single particle over a sufficiently long period (seconds) yields the same result as an ensemble measurement over a large number of particles (top panel of Figure 10b).^[59] It follows that the average of the time-series of CDSI spectra can be used to unequivocally determine the intrinsic chirality of a single nanoparticle in solution (without any geometrical artefacts). Recently, this has been demonstrated using a 200 nm long single 2-turn Au nanohelix.^[59]

Strong chiral nanoscatters also permit the observation of optical activity in nonlinear optical processes, where for instance n photons at the fundamental wavelength are annihilated to produce a single photon at the wavelength λ/n .^[172] Recently, shadow-grown chiral Ag nanohelices have permitted the observation of chiroptical effects^[60,172] that have been predicted a long time ago,^[367–369] but could not be observed with molecules. A colloidal suspension of Ag nanohelices is illuminated with a laser and the scattered light is detected (Figure 10c). This platform is currently able to observe the optical activity of higher-order harmonic scattering signals, the second ($n = 2$, Figure 10d)^[60] and third ($n = 3$) harmonics thus far.^[172] New effects and higher harmonics can possibly be detected by engineering the material complexity of the scatterers to amplify and tune their LSPR signal (shift from top to bottom in the framework in Figure 4)^[205,370] as well as their shape, for example, increasing the number of turns in the helix can enhance the chiroptical signal (shift from left to right in the framework in Figure 4).^[54] These advances in chiroptical spectroscopy with the possibility of accessing the true chiral signature of a single nanoparticle in solution promise a new robust platform for chiral sensing and spectroscopy due to the following two reasons.^[59,173,363] First, the spectroscopy of a freely diffusing nanoparticle has the advantage that the Brownian motion provides a rotationally averaged spectrum that is free from birefringence artefacts and thus a measure of the “true” chirality. In contrast, particles immobilized on a substrate can lead to additional optical artefacts, for example, linear birefringence and dichroism. This can easily mask any chiral

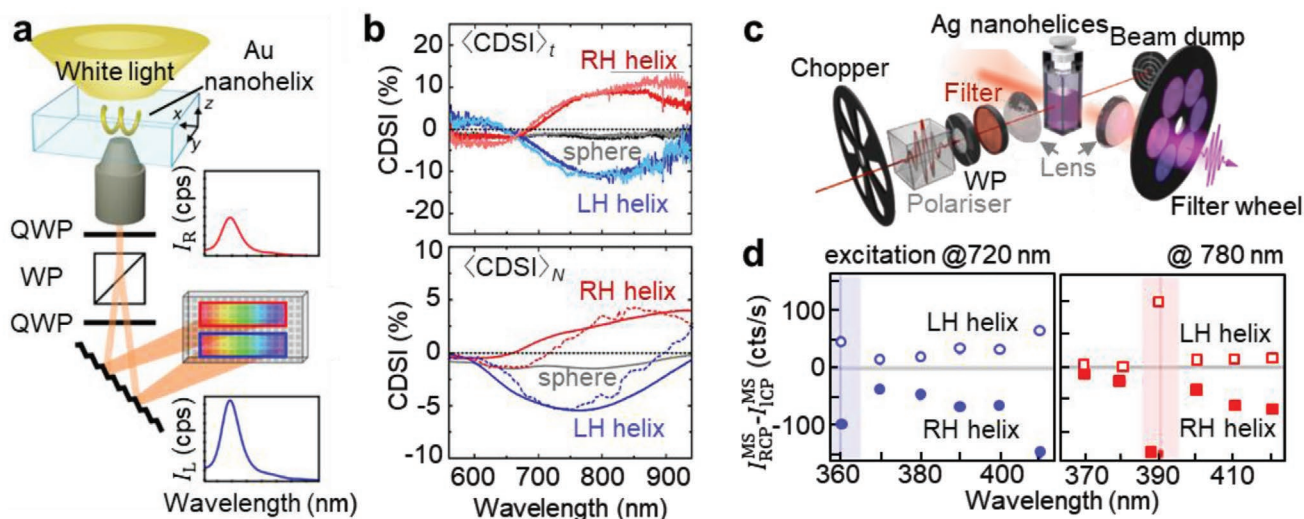


Figure 10. Single nanoparticle chiroptical spectroscopy. a) Circular differential scattering intensity, CDSI spectroscopy consisting of a dark-field condenser, quarter-wave plates (QWP), Wollaston prism (WP) polarizer, and b) measured CDSI spectra of single nanohelices averaged over time (upper) and averaged in an ensemble (lower). a, b) Reproduced under the terms of the CC-BY Creative Commons Attribution 4.0 International license (<https://creativecommons.org/licenses/by/4.0>).^[59] Copyright 2020, The Authors, published by Springer Nature. c) Nonlinear (second or third harmonic generation) chiroptical scattering spectroscopy. Reproduced under the terms of the CC-BY Creative Commons Attribution 4.0 International license (<https://creativecommons.org/licenses/by/4.0>).^[72] Copyright 2021, The Authors, published by Wiley-VCH. d) Measured spectra of second harmonic scattering intensity excited by a 720 nm (blue) and a 780 nm (red) laser. Reproduced under the terms of the CC-BY Creative Commons Attribution 4.0 International license (<https://creativecommons.org/licenses/by/4.0>).^[60] Copyright 2018, published by American Physical Society.

interactions or perturbations. Second, a low limit of detection is aided by the ability to observe a small number of nanoparticles, as the volumes are then minimal. Since measuring the plasmonic resonance of a single nanoparticle is now possible, this will aid the detection of very few analyte molecules.

6. Conclusion

PVD in the form of shadow growth, and in particular GLAD, has enabled the wafer-scale fabrication of hybrid nanostructures with nanoscale (≈ 10 nm) structural resolution, with multiple functionalities, including plasmonic, magnetic, and catalytic ones, potentially containing multiple materials and exhibiting tailored 3D shapes. Composites, alloyed, multilayered, and/or encapsulated structures can all be grown with ease. These hybrid nanostructures would be difficult to realize with any other existing method.

This review shows that increasing degrees of complexity can be achieved in the shape, ranging from highly symmetric structures to chiral ones including those without any symmetry. A feature of the shadow growth is that the structures tend to be highly uniform and that they are obtained without any chemical impurities or stabilizing molecules. In addition, we classify the hybrid nanostructures according to their material composition, which can result in Janus, core/shell, and alloyed particles (Figure 4). It is not only possible to engineer the properties of isolated nanostructures, but the same techniques also facilitate the arrangement of nanostructures, which gives rise to additional coupling phenomena. We describe nine representative structures whose shapes and compositions describe the range of systems that can be obtained as

well as the associated LSPR properties. Engineering the interactions and the environment of the plasmonic nanostructures determines the optical response across different length scales, ranging from quantum plasmonics to far-field synchronized lattice extinction effects. Furthermore, material engineering not only advances the LSPR performance used for well-established applications including spectroscopy and sensing, but also enables novel applications including for nanophotonics and robotic materials and devices. Shadow growth is particularly suited for the exploration of new complex material systems. We have further discussed how novel physical and chemical properties of hybrid plasmonic nanomaterials can be engineered and how they enable emerging applications, such as single particle chiral spectroscopy for sensing, as well as nanophotonic devices for future displays and biomedical nanorobotics.

We see a major advantage in physical shadow growth in that it facilitates the high throughput generation of novel material systems.^[37] This will enable the screening of candidate materials and structures and lends itself to combinatorial materials discovery. Material libraries of hybrid plasmonic nanomaterials will be helpful for instance in determining catalytic activity, chemical stability, or biocompatibility, where not only the composition, but also the shape are important factors that need to be considered. It will be advantageous if one at the same time also establishes standard operating procedures for nanomaterial screening and testing and if this data is shared in open-access databases. We anticipate that the nanoscale physical shadow growth will become a major tool in materials discovery and that range of exciting applications for tailored novel hybrid plasmonic nanomaterials continues to steadily increase, as it is clear that shape and materials composition underlie many important effects and properties at the nanoscale.

Acknowledgements

J.-H.H. and D.K. contributed equally to this work. The authors thank Y.M. Song for helpful comments. This work was supported by the National Research Foundation of Korea (NRF) grant funded by the Korea government (MSIT) (No. NRF-2021R1C1C1005060 and NRF-2021M3H4A1A04086552) and the DGIST R&D Program of the Ministry of Science and ICT (22-IJRP-01).

Open access funding enabled and organized by Projekt DEAL.

Conflict of Interest

The authors declare no conflict of interest.

Keywords

glancing-angle deposition, local surface plasmon resonance, nanophotonics, oblique-angle deposition, photonic nanomaterials, plasmonics, shadow growth

Received: October 3, 2021

Revised: February 23, 2022

Published online:

- [1] D. J. de Aberasturi, A. B. Serrano-Montes, L. M. Liz-Marzán, *Adv. Opt. Mater.* **2015**, *3*, 602.
- [2] D. K. Gramotnev, S. I. Bozhevolnyi, *Nat. Photonics* **2010**, *4*, 83.
- [3] K. M. Mayer, J. H. Hafner, *Chem. Rev.* **2011**, *111*, 3828.
- [4] J. A. Schuller, E. S. Barnard, W. Cai, Y. C. Jun, J. S. White, M. L. Brongersma, *Nat. Mater.* **2010**, *9*, 193.
- [5] P. K. Jain, X. Huang, I. H. El-Sayed, M. A. El-Sayed, *Acc. Chem. Res.* **2008**, *41*, 1578.
- [6] S.-W. Hsu, A. L. Rodarte, M. Som, G. Arya, A. R. Tao, *Chem. Rev.* **2018**, *118*, 3100.
- [7] N. E. Motl, A. F. Smith, C. J. DeSantis, S. E. Skrabalak, *Chem. Soc. Rev.* **2014**, *43*, 3823.
- [8] G. Baffou, C. Girard, R. Quidant, *Phys. Rev. Lett.* **2010**, *104*, 136805.
- [9] A. O. Govorov, H. H. Richardson, *Nano Today* **2007**, *2*, 30.
- [10] W. Huang, W. Qian, M. A. El-Sayed, Y. Ding, Z. L. Wang, *J. Phys. Chem. C* **2007**, *111*, 10751.
- [11] G. Baffou, F. Cichos, R. Quidant, *Nat. Mater.* **2020**, *19*, 946.
- [12] H. Kim, S. Beack, S. Han, M. Shin, T. Lee, Y. Park, K. S. Kim, A. K. Yetisen, S. H. Yun, W. Kwon, S. K. Hahn, *Adv. Mater.* **2018**, *30*, 1701460.
- [13] W. J. Parak, *Science* **2011**, *334*, 1359.
- [14] J. Gong, G. Li, Z. Tang, *Nano Today* **2012**, *7*, 564.
- [15] D. Kim, K. Shin, S. G. Kwon, T. Hyeon, *Adv. Mater.* **2018**, *30*, 1802309.
- [16] M. B. Cortie, A. M. McDonagh, *Chem. Rev.* **2011**, *111*, 3713.
- [17] C.-C. Lin, C.-W. Liao, Y.-C. Chao, C. Kuo, *ACS Appl. Mater. Interfaces* **2010**, *2*, 3185.
- [18] M. Miyata, H. Hatada, J. Takahara, *Nano Lett.* **2016**, *16*, 3166.
- [19] Z. Liu, W. R. Leow, X. Chen, *Small Methods* **2018**, *3*, 1800295.
- [20] L. Dykman, N. Khlebtsov, *Chem. Soc. Rev.* **2012**, *41*, 2256.
- [21] D. A. Giljohann, D. S. Seferos, W. L. Daniel, M. D. Massich, P. C. Patel, C. A. Mirkin, *Angew. Chem., Int. Ed.* **2010**, *49*, 3280.
- [22] T. Chen, B. M. Reinhard, *Adv. Mater.* **2016**, *28*, 3522.
- [23] M. Ha, J.-H. Kim, M. You, Q. Li, C. Fan, J.-M. Nam, *Chem. Rev.* **2019**, *119*, 12208.
- [24] E. Jeong, K. Kim, I. Choi, S. Jeong, Y. Park, H. Lee, S. H. Kim, L. P. Lee, Y. Choi, T. Kang, *Nano Lett.* **2012**, *12*, 2436.
- [25] A. G. Mark, J. G. Gibbs, T.-C. Lee, P. Fischer, *Nat. Mater.* **2013**, *12*, 802.
- [26] G. Wang, C. Hao, W. Ma, A. Qu, C. Chen, J. Xu, C. Xu, H. Kuang, L. Xu, *Adv. Mater.* **2021**, *33*, 2102337.
- [27] Y.-H. Chang, J.-W. Jang, Y.-C. Chang, S.-H. Lee, T.-F. Siao, *ACS Omega* **2020**, *5*, 14860.
- [28] H.-E. Lee, H.-Y. Ahn, J. Mun, Y. Y. Lee, M. Kim, N. H. Cho, K. Chang, W. S. Kim, J. Rho, K. T. Nam, *Nature* **2018**, *556*, 360.
- [29] M. H. Jang, J. K. Kim, H. Tak, H. Yoo, *J. Mater. Chem.* **2011**, *21*, 17606.
- [30] J. Chen, X. Gao, Q. Zheng, J. Liu, D. Meng, H. Li, R. Cai, H. Fan, Y. Ji, X. Wu, *ACS Nano* **2021**, *15*, 15114.
- [31] H. Liu, F. Nosheen, X. Wang, *Chem. Soc. Rev.* **2015**, *44*, 3056.
- [32] S. C. Glotzer, M. J. Solomon, *Nat. Mater.* **2007**, *6*, 557.
- [33] F. Laible, D. A. Gollmer, S. Dickreuter, D. P. Kern, M. Fleischer, *Nanoscale* **2018**, *10*, 14915.
- [34] P. D. Dongare, Y. Zhao, D. Renard, J. Yang, O. Neumann, J. Metz, L. Yuan, A. Alabastri, P. Nordlander, N. J. Halas, *ACS Nano* **2021**, *15*, 8761.
- [35] R. Kaissner, J. Li, W. Lu, X. Li, F. Neubrech, J. Wang, N. Liu, *Sci. Adv.* **2021**, *7*, ebd9450.
- [36] F. Qin, L. Ding, L. Zhang, F. Monticone, C. C. Chum, J. Deng, S. Mei, Y. Li, J. Teng, M. Hong, S. Zhang, A. Alù, C.-W. Qiu, *Sci. Adv.* **2016**, *2*, e1501168.
- [37] E. S. A. Goerlitz, A. S. Puri, J. J. Moses, L. V. Poulikakos, N. Vogel, *Adv. Opt. Mater.* **2021**, *9*, 2100378.
- [38] L. Y. M. Tobing, G.-Y. Goh, A. D. Mueller, L. Ke, Y. Luo, D.-H. Zhang, *Sci. Rep.* **2017**, *7*, 7539.
- [39] S. Chen, F. Zeuner, M. Weismann, B. Reineke, G. Li, V. K. Valev, K. W. Cheah, N. C. Panoiu, T. Zentgraf, S. Zhang, *Adv. Mater.* **2016**, *28*, 2992.
- [40] B. Ai, Y. Zhao, *Nanophotonics* **2019**, *8*, 1.
- [41] A. Barranco, A. Borras, A. R. Gonzalez-Elipe, A. Palmero, *Prog. Mater. Sci.* **2016**, *76*, 59.
- [42] A. B. Pawar, I. Kretzschmar, *Langmuir* **2009**, *25*, 9057.
- [43] J. G. Gibbs, *Langmuir* **2020**, *36*, 6938.
- [44] H.-H. Jeong, M. Alarcón-Correa, A. G. Mark, K. Son, T.-C. Lee, P. Fischer, *Adv. Sci.* **2017**, *4*, 1700234.
- [45] G. K. Larsen, Y. He, W. Ingram, E. T. LaPaquette, J. Wang, Y. Zhao, *Nanoscale* **2014**, *6*, 9467.
- [46] W. Yan, L. Xu, C. Xu, W. Ma, H. Kuang, L. Wang, N. A. Kotov, *J. Am. Chem. Soc.* **2012**, *134*, 15114.
- [47] N. Jiang, X. Zhuo, J. Wang, *Chem. Rev.* **2018**, *118*, 3054.
- [48] Y. He, G. K. Larsen, W. Ingram, Y. Zhao, *Nano Lett.* **2014**, *14*, 1976.
- [49] Y. He, G. Larsen, X. Li, W. Ingram, F. Chen, Y. Zhao, *Adv. Opt. Mater.* **2015**, *3*, 342.
- [50] G. K. Larsen, Y. He, W. Ingram, Y. Zhao, *Nano Lett.* **2013**, *13*, 6228.
- [51] V. M. Kadiri, C. Bussi, A. W. Holle, K. Son, H. Kwon, G. Schütz, M. G. Gutierrez, P. Fischer, *Adv. Mater.* **2020**, *32*, 2001114.
- [52] Y. Fang, R. Verre, L. Shao, P. Nordlander, M. Käll, *Nano Lett.* **2016**, *16*, 5183.
- [53] H.-H. Jeong, A. G. Mark, T.-C. Lee, M. Alarcón-Correa, S. Eslami, T. Qiu, J. G. Gibbs, P. Fischer, *Nano Lett.* **2016**, *16*, 4887.
- [54] H.-H. Jeong, A. G. Mark, M. Alarcón-Correa, I. Kim, P. Oswald, T.-C. Lee, P. Fischer, *Nat. Commun.* **2016**, *7*, 11331.
- [55] S. Larson, Y. Zhao, *J. Phys. Chem. C* **2018**, *122*, 7374.
- [56] W. Ingram, S. Larson, D. Carlson, Y. Zhao, *Nanotechnology* **2017**, *28*, 015301.
- [57] H. Kwon, S. H. Lee, J. K. Kim, *Nanoscale Res. Lett.* **2015**, *10*, 369.
- [58] Y. Liu, J. Liu, S. Sohn, Y. Li, J. J. Cha, J. Schroers, *Nat. Commun.* **2015**, *6*, 7043.

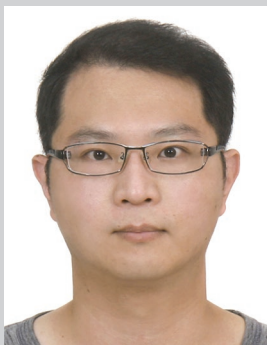
- [59] J. Sachs, J.-P. Günther, A. G. Mark, P. Fischer, *Nat. Commun.* **2020**, 11, 4513.
- [60] J. T. Collins, K. R. Rusimova, D. C. Hooper, H.-H. Jeong, L. Ohnutek, F. Pradaux-Caggiano, T. Verbiest, D. R. Carbery, P. Fischer, V. K. Valev, *Phys. Rev. X* **2019**, 9, 011024.
- [61] Y. Lin, D. Wang, J. Hu, J. Liu, W. Wang, J. Guan, R. D. Schaller, T. W. Odom, *Adv. Funct. Mater.* **2019**, 29, 1904157.
- [62] D. Bang, E.-J. Jo, S. Hong, J.-Y. Byun, J. Y. Lee, M.-G. Kim, L. P. Lee, *Nano Lett.* **2017**, 17, 6583.
- [63] S. Ghosh, A. Ghosh, *Sci. Rob.* **2018**, 3, eaaq0076.
- [64] W. He, J. Frueh, N. Hu, L. Liu, M. Gai, Q. He, *Adv. Sci.* **2016**, 3, 1600206.
- [65] A. Campos, N. Troc, E. Cottancin, M. Pellarin, H.-C. Weissker, J. Lermé, M. Kociak, M. Hillenkamp, *Nat. Phys.* **2019**, 15, 275.
- [66] M. S. Tame, K. R. McEnery, Ş. K. Özdemir, J. Lee, S. A. Maier, M. S. Kim, *Nat. Phys.* **2013**, 9, 329.
- [67] J. Olson, S. Dominguez-Medina, A. Hoggard, L.-Y. Wang, W.-S. Chang, S. Link, *Chem. Soc. Rev.* **2015**, 44, 40.
- [68] U. Kreibig, M. Vollmer, in *Optical Properties of Metal Clusters*, Vol. 25, Springer, Berlin/Heidelberg, Germany **1995**, pp. 13–201.
- [69] M. M. Miller, A. A. Lazarides, *J. Phys. Chem. B* **2005**, 109, 21556.
- [70] K.-S. Lee, M. A. El-Sayed, *J. Phys. Chem. B* **2006**, 110, 19220.
- [71] J. R. Mejía-Salazar, O. N. Oliveira Jr., *Chem. Rev.* **2018**, 118, 10617.
- [72] S. Larson, Z. Yang, Y. Zhao, *Chem. Commun.* **2019**, 55, 1342.
- [73] B. Ai, C. Song, L. Bradley, Y. Zhao, *J. Phys. Chem. C* **2018**, 122, 20935.
- [74] A. Tittl, A. Leitis, M. Liu, F. Yesilkoy, D.-Y. Choi, D. N. Neshev, Y. S. Kivshar, H. Altug, *Science* **2018**, 360, 1105.
- [75] Y. Peng, B. Xiong, L. Peng, H. Li, Y. He, E. S. Yeung, *Anal. Chem.* **2015**, 87, 200.
- [76] M. Xuan, Z. Wu, J. Shao, L. Dai, T. Si, Q. He, *J. Am. Chem. Soc.* **2016**, 138, 6492.
- [77] J. Peng, H.-H. Jeong, M. Smith, R. Chikkaraddy, Q. Lin, H.-L. Liang, M. F. L. De Volder, S. Vignolini, S. Kar-Narayan, J. J. Baumberg, *Adv. Sci.* **2021**, 8, 2002419.
- [78] F. Neubrech, X. Duan, N. Liu, *Sci. Adv.* **2020**, 6, eabc2709.
- [79] Y. He, Y. Zhao, *Nanoscale* **2011**, 3, 2361.
- [80] W. Qin, T. Peng, Y. Gao, F. Wang, X. Hu, K. Wang, J. Shi, D. Li, J. Ren, C. Fan, *Angew. Chem., Int. Ed.* **2017**, 56, 515.
- [81] A. N. Koya, X. Zhu, N. Ohannesian, A. A. Yanik, A. Alabastri, R. P. Zaccaria, R. Krahne, W.-C. Shih, D. Garoli, *ACS Nano* **2021**, 15, 6038.
- [82] M. Matuschek, D. P. Singh, H.-H. Jeong, M. Nesterov, T. Weiss, P. Fischer, F. Neubrech, N. Liu, *Small* **2018**, 14, 1702990.
- [83] K. T. Hong, C. W. Moon, J. M. Suh, T. H. Lee, S.-I. Kim, S. Lee, H. W. Jang, *ACS Appl. Mater. Interfaces* **2019**, 11, 11568.
- [84] *Thin Film Processes II* (Ed: J. L. Vossen, W. Kern), Vol. 2, Elsevier, London, UK **2012**.
- [85] J. E. Crowell, *J. Vac. Sci. Technol., A* **2003**, 21, S88.
- [86] K. F. Jensen, in *Microelectronics Processing: Chemical Engineering Aspects* (Eds: D. W. Hess, K. F. Jensen), American Chemical Society, Washington, DC, USA **1989**, pp. 199–263.
- [87] M. Chen, R. C. Haddon, R. Yan, E. Bekyarova, *Mater. Horiz.* **2017**, 4, 1054.
- [88] Z. Cai, Y. Lai, S. Zhao, R. Zhang, J. Tan, S. Feng, J. Zou, L. Tang, J. Lin, B. Liu, H.-M. Cheng, *Natl. Sci. Rev.* **2021**, 8, nwaa115.
- [89] P.-C. Shen, Y. Lin, H. Wang, J.-H. Park, W. S. Leong, A.-Y. Lu, T. Palacios, J. Kong, *IEEE Trans. Electron Devices* **2018**, 65, 4040.
- [90] Y. Wang, X. Guan, D. Li, H.-C. Cheng, X. Duan, Z. Lin, X. Duan, *Nano Res.* **2017**, 10, 1223.
- [91] Z. Cai, B. Liu, X. Zou, H.-M. Cheng, *Chem. Rev.* **2018**, 118, 6091.
- [92] M. Wang, M. Huang, D. Luo, Y. Li, M. Choe, W. K. Seong, M. Kim, S. Jin, M. Wang, S. Chatterjee, Y. Kwon, Z. Lee, R. S. Ruoff, *Nature* **2021**, 596, 519.
- [93] X. Fan, T. Chen, L. Dai, *RSC Adv.* **2014**, 4, 36996.
- [94] B. N. Chandrashekar, B. Deng, A. S. Smitha, Y. Chen, C. Tan, H. Zhang, H. Peng, Z. Liu, *Adv. Mater.* **2015**, 27, 5210.
- [95] T. Das, B. K. Sharma, A. K. Katiyar, J.-H. Ahn, *J. Semicond.* **2018**, 39, 011007.
- [96] K. Rana, J. Singh, J.-H. Ahn, *J. Mater. Chem. C* **2014**, 2, 2646.
- [97] Q. Zeng, Z. Liu, *Adv. Electron. Mater.* **2018**, 4, 1700335.
- [98] Z. Huang, F. Bai, *Nanoscale* **2014**, 6, 9401.
- [99] G. K. Larsen, Y. He, J. Wang, Y. Zhao, *Adv. Opt. Mater.* **2014**, 2, 245.
- [100] H.-H. Jeong, A. G. Mark, J. G. Gibbs, T. Reindl, U. Waizmann, J. Weis, P. Fischer, *Nanotechnology* **2014**, 25, 235302.
- [101] H. König, G. Helwig, *Optik* **1950**, 6, 111.
- [102] N. O. Young, J. Kowal, *Nature* **1959**, 183, 104.
- [103] K. Robbie, M. J. Brett, A. Lakhtakia, *Nature* **1996**, 384, 616.
- [104] B. Gallas, N. Guth, J. Rivory, H. Arwin, R. Magnusson, G. Guida, J. Yang, K. Robbie, *Thin Solid Films* **2011**, 519, 2650.
- [105] H.-N. Barad, H. Kwon, M. Alarcón-Correa, P. Fischer, *ACS Nano* **2021**, 15, 5861.
- [106] S. Aksu, A. A. Yanik, R. Adato, A. Artar, M. Huang, H. Altug, *Nano Lett.* **2010**, 10, 2511.
- [107] F. Hong, R. Blaikie, *Adv. Opt. Mater.* **2019**, 7, 1801653.
- [108] S. Dickreuter, J. Gleixner, A. Kolloch, J. Boneberg, E. Scheer, P. Leiderer, *Beilstein J. Nanotechnol.* **2013**, 4, 588.
- [109] Y. Yu, G. Zhang, in *Updates in Advanced Lithography* (Ed: S. Hosaka), IntechOpen, London, UK **2013**, Ch. 1.
- [110] Z. Li, A. Lopez-Ortega, A. Aranda-Ramos, J. L. Tajada, J. Sort, C. Nogues, P. Vavassori, J. Nogues, B. Sepulveda, *Small* **2018**, 14, 1800868.
- [111] Y. Qu, Z. Zhang, T. Fu, G. Wang, T. Wang, M. Wang, Y. Bai, Z. Zhang, *J. Phys. D: Appl. Phys.* **2017**, 50, 504001.
- [112] L. Bradley, D. Ye, H. M. Luong, Y. Zhao, *Nanotechnology* **2020**, 31, 205301.
- [113] D. Paria, K. Roy, H. J. Singh, S. Kumar, S. Raghavan, A. Ghosh, A. Ghosh, *Adv. Mater.* **2015**, 27, 1751.
- [114] A. Kosiorek, W. Kandulski, P. Chudzinski, K. Kempa, M. Giersig, *Nano Lett.* **2004**, 4, 1359.
- [115] J. Zhao, B. Frank, S. Burger, H. Giessen, *ACS Nano* **2011**, 5, 9009.
- [116] J. C. Hulst, R. P. Van Duyne, *J. Vac. Sci. Technol., A* **1995**, 13, 1553.
- [117] V. E. Bochenkov, D. S. Sutherland, *Nano Lett.* **2013**, 13, 1216.
- [118] M. C. Gwinner, E. Koroknay, L. Fu, P. Patoka, W. Kandulski, M. Giersig, H. Giessen, *Small* **2009**, 5, 400.
- [119] V. E. Bochenkov, D. S. Sutherland, *Opt. Express* **2018**, 26, 27101.
- [120] B. Frank, X. Yin, M. Schäferling, J. Zhao, S. M. Hein, P. V. Braun, H. Giessen, *ACS Nano* **2013**, 7, 6321.
- [121] R. Glass, M. M. Möller, J. P. Spatz, *Nanotechnology* **2003**, 14, 1153.
- [122] H.-H. Jeong, A. G. Mark, T.-C. Lee, K. Son, W. Chen, M. Alarcón-Correa, I. Kim, G. Schütz, P. Fischer, *Adv. Sci.* **2015**, 2, 1500016.
- [123] J. G. Gibbs, A. G. Mark, T.-C. Lee, S. Eslami, D. Schamel, P. Fischer, *Nanoscale* **2014**, 6, 9457.
- [124] T. Lohmueller, E. Bock, J. P. Spatz, *Adv. Mater.* **2008**, 20, 2297.
- [125] S. Goy-López, E. Castro, P. Taboada, V. Mosquera, *Langmuir* **2008**, 24, 13186.
- [126] H.-H. Jeong, M. C. Adams, J. P. Günther, M. Alarcón-Correa, I. Kim, E. Choi, C. Miksch, A. F. Mark, A. G. Mark, P. Fischer, *ACS Nano* **2019**, 13, 11453.
- [127] H.-H. Jeong, A. G. Mark, J. G. Gibbs, T. Reindl, U. Waizmann, J. Weis, P. Fischer, in *2014 IEEE 27th Int. Conf. on Micro Electro Mechanical Systems (MEMS)*, IEEE, Piscataway, NJ, USA **2014**, pp. 437–440, <https://doi.org/10.1109/MEMSYS.2014.6765670>.
- [128] B. A. Movchan, A. V. Demchishin, *Fiz. Met. Metalloved.* **1969**, 28, 653.
- [129] P. B. Barna, M. Adamik, *Thin Solid Films* **1998**, 317, 27.
- [130] S. Mukherjee, D. Gall, *Thin Solid Films* **2013**, 527, 158.

- [131] C. M. Maier, M. A. Huergo, S. Milosevic, C. Pernpeintner, M. Li, D. P. Singh, D. Walker, P. Fischer, J. Feldmann, T. Lohmüller, *Nano Lett.* **2018**, *18*, 7935.
- [132] R. Ogier, Y. Fang, M. Svedendahl, P. Johansson, M. Käll, *ACS Photonics* **2014**, *1*, 1074.
- [133] E. S. A. Goerlitz, R. Mohammadi, S. Nechayev, K. Volk, M. Rey, P. Banzer, M. Karg, N. Vogel, *Adv. Mater.* **2020**, *32*, 2001330.
- [134] W.-F. Lau, L. Yang, F. Bai, Z. Huang, *Small* **2016**, *12*, 6698.
- [135] W. Lu, N. Jiang, J. Wang, *Adv. Mater.* **2017**, *29*, 1604862.
- [136] J. Peng, H.-H. Jeong, Q. Lin, S. Cormier, H.-L. Liang, M. F. L. De Volder, S. Vignolini, J. J. Baumberg, *Sci. Adv.* **2019**, *5*, eaaw2205.
- [137] I. Pastoriza-Santos, C. Kinnear, J. Pérez-Juste, P. Mulvaney, L. M. Liz-Marzán, *Nat. Rev. Mater.* **2018**, *3*, 375.
- [138] W. Smith, A. Wolcott, R. C. Fitzmorris, J. Z. Zhang, Y. Zhao, *J. Mater. Chem.* **2011**, *21*, 10792.
- [139] Y.-J. Oh, S.-G. Park, M.-H. Kang, J.-H. Choi, Y. Nam, K.-H. Jeong, *Small* **2011**, *7*, 184.
- [140] D. P. Singh, R. Nagar, J. P. Singh, *J. Appl. Phys.* **2010**, *107*, 074306.
- [141] S. Venkataramanababu, G. Nair, P. Deshpande, J. M. A. S. Mohan, A. Ghosh, *Nanotechnology* **2018**, *29*, 255203.
- [142] H. Johnson Singh, A. Ghosh, *J. Phys. Chem. C* **2012**, *116*, 19467.
- [143] C. J. DeSantis, S. E. Skrabalak, *Langmuir* **2012**, *28*, 9055.
- [144] W. Huang, F. Yang, L. Zhu, R. Qiao, Y. Zhao, *Soft Matter* **2017**, *13*, 3750.
- [145] P. L. Venugopalan, R. Sai, Y. Chandorkar, B. Basu, S. Shivashankar, A. Ghosh, *Nano Lett.* **2014**, *14*, 1968.
- [146] V. M. Kadiri, J.-P. Günther, S. N. Kottapalli, R. Goyal, F. Peter, M. Alarcón-Correa, K. Son, H.-N. Barad, M. Börsch, P. Fischer, *Eur. Phys. J. E: Soft Matter Biol. Phys.* **2021**, *44*, 74.
- [147] Z. Wu, J. Troll, H.-H. Jeong, Q. Wei, M. Stang, F. Ziemssen, Z. Wang, M. Dong, S. Schnichels, T. Qiu, P. Fischer, *Sci. Adv.* **2018**, *4*, eaat4388.
- [148] N. Lee, J. Kwak, J. H. Kwak, S.-M. Jung, J. Kim, A. Giri, K. Thiyagarajan, Y.-T. Kim, S. Jung, J. K. Kim, U. Jeong, *J. Mater. Chem. A* **2020**, *8*, 9654.
- [149] J. Kim, H. Jung, S.-M. Jung, J. Hwang, D. Y. Kim, N. Lee, K.-S. Kim, H. Kwon, Y.-T. Kim, J. W. Han, J. K. Kim, *J. Am. Chem. Soc.* **2021**, *143*, 1399.
- [150] H. Savaloni, A. Esfandiari, *Appl. Surf. Sci.* **2011**, *257*, 9425.
- [151] M. S. Rodrigues, J. Borges, M. Proença, P. Pedrosa, N. Martin, K. Romanyuk, A. L. Kholkin, F. Vaz, *Nanotechnology* **2019**, *30*, 225701.
- [152] Y. He, X. Wang, W. Ingram, B. Ai, Y. Zhao, *Nanotechnology* **2018**, *29*, 165301.
- [153] Y. Wang, J. Deng, G. Wang, T. Fu, Y. Qu, Z. Zhang, *Opt. Express* **2016**, *24*, 2307.
- [154] V. G. Kravets, A. V. Kabashin, W. L. Barnes, A. N. Grigorenko, *Chem. Rev.* **2018**, *118*, 5912.
- [155] H. Tang, C.-J. Chen, Z. Huang, J. Bright, G. Meng, R.-S. Liu, N. Wu, *J. Chem. Phys.* **2020**, *152*, 220901.
- [156] A. Furube, S. Hashimoto, *NPG Asia Mater.* **2017**, *9*, e454.
- [157] M. L. Brongersma, N. J. Halas, P. Nordlander, *Nat. Nanotechnol.* **2015**, *10*, 25.
- [158] H. Kang, W. Hong, Y. An, S. Yoo, H.-J. Kwon, Y. Nam, *ACS Nano* **2020**, *14*, 11406.
- [159] J. D. Dove, T. W. Murray, M. A. Borden, *Soft Matter* **2013**, *9*, 7743.
- [160] C. Tao, L. An, J. Lin, Q. Tian, S. Yang, *Small* **2019**, *15*, 1903473.
- [161] Y. Mantri, J. V. Jokerst, *ACS Nano* **2020**, *14*, 9408.
- [162] R. Verre, M. Svedendahl, N. O. Länk, Z. J. Yang, G. Zengin, T. J. Antosiewicz, M. Käll, *Nano Lett.* **2016**, *16*, 98.
- [163] M. Kim, J.-H. Lee, J.-M. Nam, *Adv. Sci.* **2019**, *6*, 1900471.
- [164] J.-E. Park, M. Kim, J.-H. Hwang, J.-M. Nam, *Small Methods* **2017**, *1*, 1600032.
- [165] Y. Liu, M. Yang, J. Zhang, X. Zhi, C. Li, C. Zhang, F. Pan, K. Wang, Y. Yang, J. M. de la Fuentea, D. Cui, *ACS Nano* **2016**, *10*, 2375.
- [166] L. Tong, J.-X. Cheng, *Mater. Today* **2011**, *14*, 264.
- [167] A. M. Goodman, N. J. Hogan, S. Gottheim, C. Li, S. E. Clare, N. J. Halas, *ACS Nano* **2017**, *11*, 171.
- [168] J. Lin, S. Wang, P. Huang, Z. Wang, S. Chen, G. Niu, W. Li, J. He, D. Cui, G. Lu, X. Chen, Z. Nie, *ACS Nano* **2013**, *7*, 5320.
- [169] J. Mun, M. Kim, Y. Yang, T. Badloe, J. Ni, Y. Chen, C.-W. Qiu, J. Rho, *Light: Sci. Appl.* **2020**, *9*, 139.
- [170] X. Yin, M. Schäferling, B. Metzger, H. Giessen, *Nano Lett.* **2013**, *13*, 6238.
- [171] J. T. Collins, C. Kuppe, D. C. Hooper, C. Sibilia, M. Centini, V. K. Valev, *Adv. Opt. Mater.* **2017**, *5*, 1700182.
- [172] L. Ohnouteck, H.-H. Jeong, R. R. Jones, J. Sachs, B. J. Olohan, D.-M. Rășădean, G. D. Pantoș, D. L. Andrews, P. Fischer, V. K. Valev, *Laser Photonics Rev.* **2021**, *15*, 2100235.
- [173] J. Karst, N. Strohfeldt, M. Schäferling, H. Giessen, M. Hentschel, *Adv. Opt. Mater.* **2018**, *6*, 1800087.
- [174] Y. Min, Y. Wang, *Front. Chem.* **2020**, *8*, 411.
- [175] H. Zhang, C. Wang, H. Li, L. Jiang, D. Men, J. Wang, J. Xiang, *RSC Adv.* **2018**, *8*, 9134.
- [176] M. Sui, S. Kunwar, P. Pandey, J. Lee, *Sci. Rep.* **2019**, *9*, 16582.
- [177] R. Ogier, Y. Fang, M. Käll, M. Svedendahl, *Phys. Rev. X* **2015**, *5*, 041019.
- [178] M.-S. Noh, S. D. Han, S. Chae, S. H. Back, S. Kim, S.-H. Baek, S. K. Kim, J.-W. Choi, J.-S. Kim, D. J. Ahn, D. Choi, C.-Y. Kang, *J. Mater. Chem. C* **2018**, *6*, 6038.
- [179] R. Ogier, L. Shao, M. Svedendahl, M. Käll, *Adv. Mater.* **2016**, *28*, 4658.
- [180] M. C. Giordano, A. Foti, E. Messina, P. G. Gucciardi, D. Comoretto, F. B. de Mongeot, *ACS Appl. Mater. Interfaces* **2016**, *8*, 6629.
- [181] Y.-J. Jen, S. Chan, J.-W. Huang, C.-Y. Jheng, W.-C. Liu, *Nanoscale Res. Lett.* **2015**, *10*, 498.
- [182] M. Zhang, N. Large, A. L. Koh, Y. Cao, A. Manjavacas, R. Sinclair, P. Nordlander, S. X. Wang, *ACS Nano* **2015**, *9*, 9331.
- [183] S. Abbasian, A. Moshaii, N. S. Vayghan, M. Nikkha, *Appl. Surf. Sci.* **2018**, *441*, 613.
- [184] L. Yang, C.-S. Kwan, L. Zhang, X. Li, Y. Han, K. C.-F. Leung, Y. Yang, Z. Huang, *Adv. Funct. Mater.* **2019**, *29*, 1807307.
- [185] A. Taghavi, F. Rahbarizadeh, S. Abbasian, A. Moshaii, *Plasmonics* **2020**, *15*, 753.
- [186] P. Goel, K. Singh, J. P. Singh, *RSC Adv.* **2014**, *4*, 11130.
- [187] Y. S. Jung, Z. Sun, H. K. Kim, *Appl. Phys. Lett.* **2005**, *87*, 263116.
- [188] D. A. Gish, F. Nsiah, M. T. McDermott, M. J. Brett, *Anal. Chem.* **2007**, *79*, 4228.
- [189] F. Cuccureddu, S. Murphy, I. V. Shvets, M. Porcu, H. W. Zandbergen, *Nano Lett.* **2008**, *8*, 3248.
- [190] X. Wei, J. Liu, G.-J. Xia, J. Deng, P. Sun, J. J. Churma, W. Wu, C. Yang, Y.-G. Wang, Z. Huang, *Nat. Chem.* **2020**, *12*, 551.
- [191] J. H. Singh, G. Nair, A. Ghosh, A. Ghosh, *Nanoscale* **2013**, *5*, 7224.
- [192] S. Kim, J.-M. Kim, J.-E. Park, J.-M. Nam, *Adv. Mater.* **2018**, *30*, 1704528.
- [193] J. M. Caridad, C. Tserkezis, J. E. Santos, P. Plochocka, M. Venkatesan, J. M. D. Coey, N. A. Mortensen, G. L. J. A. Rikken, V. Krstić, *Phys. Rev. Lett.* **2021**, *126*, 177401.
- [194] H.-H. Jeong, A. G. Mark, P. Fischer, *Chem. Commun.* **2016**, *52*, 12179.
- [195] R. B. Abdulrahman, H. Cansizoglu, M. F. Cansizoglu, J. B. Herzog, T. Karabacak, *J. Vac. Sci. Technol., A* **2015**, *33*, 041501.
- [196] S. Balbinot, A. M. Srivastav, J. Vidic, I. Abdulhalim, M. Manzano, *Trends Food Sci. Technol.* **2021**, *111*, 128.
- [197] S. Y. Oh, N. S. Heo, S. Shukla, H.-J. Cho, A. T. E. Vilian, J. Kim, S. Y. Lee, Y.-K. Han, S. M. Yoo, Y. S. Huh, *Sci. Rep.* **2017**, *7*, 10130.

- [198] S. Jayabal, A. Pandikumar, H. N. Lim, R. Ramaraj, T. Sun, N. M. Huang, *Analyst* **2015**, *140*, 2540.
- [199] S. B. D. Borah, T. Bora, S. Baruah, J. Dutta, *Groundwater Sustainable Dev.* **2015**, *1*, 1.
- [200] C.-Y. Chang, H.-T. Lin, M.-S. Lai, T.-Y. Shieh, C.-C. Peng, M.-H. Shih, Y.-C. Tung, *Sci. Rep.* **2018**, *8*, 11812.
- [201] C. M. Das, Y. Guo, G. Yang, L. Kang, G. Xu, H.-P. Ho, K.-T. Yong, *Adv. Theory Simul.* **2020**, *3*, 2000185.
- [202] A. R. Ferhan, Y. Hwang, M. S. B. Ibrahim, S. Anand, A. Kim, J. A. Jackman, N.-J. Cho, *Appl. Mater. Today* **2021**, *23*, 101046.
- [203] H. Chen, X. Kou, Z. Yang, W. Ni, J. Wang, *Langmuir* **2008**, *24*, 5233.
- [204] R. Liu, J.-H. Zhou, Z.-K. Zhou, X. Jiang, J. Liu, G. Liu, X.-H. Wang, *Nanoscale* **2014**, *6*, 13145.
- [205] H.-H. Jeong, E. Choi, E. Ellis, T.-C. Lee, *J. Mater. Chem. B* **2019**, *7*, 3480.
- [206] J. Homola, M. Piliarik, in *Surface Plasmon Resonance Based Sensors*, Springer, Berlin/Heidelberg, Germany **2006**, pp. 45–67.
- [207] T. G. Habteyes, S. Dhuey, E. Wood, D. Gargas, S. Cabrini, P. J. Schuck, A. P. Alivisatos, S. R. Leone, *ACS Nano* **2012**, *6*, 5702.
- [208] J. Liu, B. Cankurtaran, L. Wiczorek, M. J. Ford, M. Cortie, *Adv. Funct. Mater.* **2006**, *16*, 1457.
- [209] Y. He, Z. Zhang, C. Hoffmann, Y. Zhao, *Adv. Funct. Mater.* **2008**, *18*, 1676.
- [210] T. Fu, Y. Qu, T. Wang, G. Wang, Y. Wang, H. Li, J. Li, L. Wang, Z. Zhang, *J. Phys. Chem. C* **2017**, *121*, 1299.
- [211] S. Ghosh, A. Ghosh, *Nat. Commun.* **2019**, *10*, 4191.
- [212] Y. Hou, S. Li, Y. Su, X. Huang, Y. Liu, L. Huang, Y. Yu, F. Gao, Z. Zhang, *J. Du, Langmuir* **2013**, *29*, 867.
- [213] Y. Hou, H. M. Leung, C. T. Chan, J. Du, H. L.-W. Chan, D. Y. Lei, *Adv. Funct. Mater.* **2016**, *26*, 7807.
- [214] L. Bradley, Y. Zhao, *Langmuir* **2016**, *32*, 4969.
- [215] D. Paria, H.-H. Jeong, V. Vadakkumbatt, P. Deshpande, P. Fischer, A. Ghosh, A. Ghosh, *Nanoscale* **2018**, *10*, 7685.
- [216] J. Liu, Z. Ni, P. Nandi, U. Mirsaidov, Z. Huang, *Nano Lett.* **2019**, *19*, 7427.
- [217] J. G. Gibbs, A. G. Mark, S. Eslami, P. Fischer, *Appl. Phys. Lett.* **2013**, *103*, 213101.
- [218] H. M. Luong, M. T. Pham, T. D. Nguyen, Y. Zhao, *Nanotechnology* **2019**, *30*, 425203.
- [219] H. Yin, Z. Ma, M. Chi, S. Dai, *Catal. Today* **2011**, *160*, 87.
- [220] H.-x. Shen, J.-l. Yao, R.-a. Gu, *Trans. Nonferrous Met. Soc. China* **2009**, *19*, 652.
- [221] A. Tittl, P. Mai, R. Taubert, D. Dregely, N. Liu, H. Giessen, *Nano Lett.* **2011**, *11*, 4366.
- [222] R. Griessen, N. Strohfeldt, H. Giessen, *Nat. Mater.* **2016**, *15*, 311.
- [223] A. Baldi, T. C. Narayan, A. L. Koh, J. A. Dionne, *Nat. Mater.* **2014**, *13*, 1143.
- [224] P. B. Johnson, R. W. Christy, *Phys. Rev. B* **1972**, *6*, 4370.
- [225] P. B. Johnson, R. W. Christy, *Phys. Rev. B* **1974**, *9*, 5056.
- [226] M. J. Dodge, *Appl. Opt.* **1984**, *23*, 1980.
- [227] J. J. Mock, D. R. Smith, S. Schultz, *Nano Lett.* **2003**, *3*, 485.
- [228] A. D. McFarland, R. P. Van Duyne, *Nano Lett.* **2003**, *3*, 1057.
- [229] D. E. Charles, D. Aherne, M. Gara, D. M. Ledwith, Y. K. Gun'ko, J. M. Kelly, W. J. Blau, M. E. Brennan-Fournet, *ACS Nano* **2010**, *4*, 55.
- [230] L. J. Sherry, R. Jin, C. A. Mirkin, G. C. Schatz, R. P. Van Duyne, *Nano Lett.* **2006**, *6*, 2060.
- [231] C. L. Nehl, H. Liao, J. H. Hafner, *Nano Lett.* **2006**, *6*, 683.
- [232] S. K. Dondapati, T. K. Sau, C. Hrelescu, T. A. Klar, F. D. Stefani, J. Feldmann, *ACS Nano* **2010**, *4*, 6318.
- [233] R. M. Pallares, T. Stilson, P. Choo, J. Hu, T. W. Odom, *ACS Appl. Nano Mater.* **2019**, *2*, 5266.
- [234] Z. J. Woessner, A. N. Chen, S. E. Skrabalak, *J. Phys. Chem. C* **2021**, *125*, 11262.
- [235] L. J. Sherry, S.-H. Chang, G. C. Schatz, R. P. Van Duyne, B. J. Wiley, Y. Xia, *Nano Lett.* **2005**, *5*, 2034.
- [236] W. J. Galush, S. A. Shelby, M. J. Mulvihill, A. Tao, P. Yang, J. T. Groves, *Nano Lett.* **2009**, *9*, 2077.
- [237] H. R. Hegde, S. Chidangil, R. K. Sinha, *RSC Adv.* **2021**, *11*, 8042.
- [238] F. Tam, C. Moran, N. Halas, *J. Phys. Chem. B* **2004**, *108*, 17290.
- [239] Y. Sun, Y. Xia, *Anal. Chem.* **2002**, *74*, 5297.
- [240] H. Wang, D. W. Brandl, F. Le, P. Nordlander, N. J. Halas, *Nano Lett.* **2006**, *6*, 827.
- [241] G. Raschke, A. S. Brogl, A. S. Susa, A. L. Rogach, T. A. Klar, J. Feldmann, B. Fieres, N. Petkov, T. Bein, A. Nichtl, K. Kürzinger, *Nano Lett.* **2004**, *4*, 1853.
- [242] N. Zhou, C. Ye, L. Polavarapu, Q.-H. Xu, *Nanoscale* **2015**, *7*, 9025.
- [243] Y. He, K. Lawrence, W. Ingram, Y. Zhao, *Chem. Commun.* **2016**, *52*, 2047.
- [244] A. K. Ghosh, S. Sarkar, L. J. Nebel, O. Aftenieva, V. Gupta, O. Sander, A. Das, J. Joseph, S. Wiefner, T. A. F. König, A. Fery, *Adv. Funct. Mater.* **2021**, *31*, 2101959.
- [245] S. Chen, E. S. H. Kang, M. S. Chaharsoughi, V. Stanishev, P. Kühne, H. Sun, C. Wang, M. Fahlman, S. Fabiano, V. Darakchieva, M. P. Jonsson, *Nat. Nanotechnol.* **2020**, *15*, 35.
- [246] M. Atighiorestani, H. Jiang, B. Kaminska, *Adv. Opt. Mater.* **2018**, *6*, 1801179.
- [247] W. Lu, T. H. Chow, Y. Lu, J. Wang, *Nanoscale* **2020**, *12*, 21617.
- [248] J. Ratzsch, J. Karst, J. Fu, M. Ubl, T. Pohl, F. Sterl, C. Malacrida, M. Wieland, B. Reineke, T. Zentgraf, S. Ludwigs, M. Hentschel, H. Giessen, *J. Opt.* **2020**, *22*, 124001.
- [249] M. Gugole, O. Olsson, K. Xiong, J. C. Blake, J. Montero Amenedo, I. Bayrak Pehlivan, G. A. Niklasson, A. Dahlin, *ACS Photonics* **2020**, *7*, 1762.
- [250] M. Gugole, O. Olsson, S. Rossi, M. P. Jonsson, A. Dahlin, *Nano Lett.* **2021**, *21*, 4343.
- [251] L. Shao, X. Zhuo, J. Wang, *Adv. Mater.* **2018**, *30*, 1704338.
- [252] K. Xiong, D. Tordera, M. P. Jonsson, A. B. Dahlin, *Rep. Prog. Phys.* **2019**, *82*, 024501.
- [253] R. W. Taylor, T.-C. Lee, O. A. Scherman, R. Esteban, J. Aizpurua, F. M. Huang, J. J. Baumberg, S. Mahajan, *ACS Nano* **2011**, *5*, 3878.
- [254] W. Zhu, R. Esteban, A. G. Borisov, J. J. Baumberg, P. Nordlander, H. J. Lezec, J. Aizpurua, K. B. Crozier, *Nat. Commun.* **2016**, *7*, 11495.
- [255] B. Felix, K. M. Schmidt, L. Dreismann, R. Chikkaraddy, Y. Zhang, A. Demetriadou, C. Carnegie, H. Ohadi, B. De Nijs, R. Esteban, J. Aizpurua, J. J. Baumberg, *Science* **2016**, *354*, 726.
- [256] S. Schlücker, *Angew. Chem., Int. Ed.* **2014**, *53*, 4756.
- [257] V. K. Valev, J. J. Baumberg, C. Sibilia, T. Verbiest, *Adv. Mater.* **2013**, *25*, 2517.
- [258] I. Ragheb, M. Braik, A. Mezeghrane, L. Boubekeur-Lecaque, A. Belkhir, N. Felidj, *J. Opt. Soc. Am. B* **2019**, *36*, E36.
- [259] V. Giannini, G. Vecchi, J. G. Rivas, *Phys. Rev. Lett.* **2010**, *105*, 266801.
- [260] A. I. Väkeväinen, R. J. Moerland, H. T. Rekola, A.-P. Eskelinen, J.-P. Martikainen, D.-H. Kim, P. Törmä, *Nano Lett.* **2014**, *14*, 1721.
- [261] M. S. Bin-Alam, O. Reshef, Y. Mamchur, M. Z. Alam, G. Carlow, J. Upham, B. T. Sullivan, J.-M. Ménard, M. J. Huttunen, R. W. Boyd, K. Dolgaleva, *Nat. Commun.* **2021**, *12*, 974.
- [262] X. Zhu, G. M. Imran Hossain, M. George, A. Farhang, A. Cicek, A. A. Yanik, *ACS Photonics* **2020**, *7*, 416.
- [263] L. Y. M. Tobing, A. M. Soehartono, A. D. Mueller, K.-T. Yong, W. Fan, D. H. Zhang, *Nanoscale* **2021**, *13*, 4092.
- [264] K. Yang, X. Yao, B. Liu, B. Ren, *Adv. Mater.* **2021**, *33*, 2007988.
- [265] D. Wang, M. R. Bourgeois, W.-K. Lee, R. Li, D. Trivedi, M. P. Knudson, W. Wang, G. C. Schatz, T. W. Odom, *Nano Lett.* **2018**, *18*, 4549.
- [266] J. Guan, R. Li, X. G. Juarez, A. D. Sample, Y. Wang, G. C. Schatz, T. W. Odom, *Adv. Mater.* **2021**, <https://doi.org/10.1002/adma.202103262>

- [267] L. Wang, M. Hasanzadeh Kafshgari, M. Meunier, *Adv. Funct. Mater.* **2020**, 30, 2005400.
- [268] J. Mosquera, Y. Zhao, H.-J. Jang, N. Xie, C. Xu, N. A. Kotov, L. M. Liz-Marzán, *Adv. Funct. Mater.* **2020**, 30, 1902082.
- [269] M. Alqahtani, A. Kafizas, S. Sathasivam, M. Ebaid, F. Cui, A. Alyamani, H.-H. Jeong, T. C. Lee, P. Fischer, I. Parkin, M. Grätzel, J. Wu, *ChemSusChem* **2020**, 13, 6028.
- [270] Q. Shi, D. Sikdar, R. Fu, K. J. Si, D. Dong, Y. Liu, M. Premaratne, W. Cheng, *Adv. Mater.* **2018**, 30, 1801118.
- [271] Y. Jung, H. Jung, H. Choi, H. Lee, *Nano Lett.* **2020**, 20, 6344.
- [272] X. Wang, C. Dai, X. Yao, T. Qiao, M. Chen, S. Li, Z. Shi, M. Wang, Z. Huang, X. Hu, Z. Li, J. Zhang, X. Zhang, *Nanoscale* **2021**, 13, 7273.
- [273] B. Chen, A. Wood, A. Pathak, J. Mathai, S. Bok, H. Zheng, S. Hamm, S. Basuray, S. Grant, K. Gangopadhyay, P. V. Cornish, S. Gangopadhyay, *Nanoscale* **2016**, 8, 12189.
- [274] X. Chen, M. Chen, M. Q. Mehmood, D. Wen, F. Yue, C.-W. Qiu, S. Zhang, *Adv. Opt. Mater.* **2015**, 3, 1201.
- [275] J. H. Ko, Y. J. Yoo, Y. J. Kim, S.-S. Lee, Y. M. Song, *Adv. Funct. Mater.* **2020**, 30, 1908592.
- [276] Y.-J. Lu, T. L. Shen, K.-N. Peng, P.-J. Cheng, S.-W. Chang, M.-Y. Lu, C. W. Chu, T.-F. Guo, H. A. Atwater, *ACS Photonics* **2021**, 8, 335.
- [277] Z. Zhang, Y. Liu, Y. Fang, B. Cao, J. Huang, K. Liu, B. Dong, *Adv. Sci.* **2018**, 5, 1800748.
- [278] Y. Liang, C. Li, Y.-Z. Huang, Q. Zhang, *ACS Nano* **2020**, 14, 14375.
- [279] Q. Zhang, Q. Shang, J. Shi, J. Chen, R. Wang, Y. Mi, W. Du, C. Shen, R. Ma, X. Qiu, X. Liu, T. C. Sum, *ACS Photonics* **2017**, 4, 2789.
- [280] Y. Wang, J. Yu, Y.-F. Mao, J. Chen, S. Wang, H.-Z. Chen, Y. Zhang, S.-Y. Wang, X. Chen, T. Li, L. Zhou, R.-M. Ma, S. Zhu, W. Cai, J. Zhu, *Nature* **2020**, 581, 401.
- [281] J. W. Lee, G. Ha, J. Park, H. G. Song, J. Y. Park, J. Lee, Y.-H. Cho, J.-L. Lee, J. K. Kim, J. K. Kim, *ACS Appl. Mater. Interfaces* **2020**, 12, 36339.
- [282] P. Mao, C. Liu, X. Li, M. Liu, Q. Chen, M. Han, S. A. Maier, E. H. Sargent, S. Zhang, *Light: Sci. Appl.* **2021**, 10, 180.
- [283] W.-J. Joo, J. Kyoung, M. Esfandyarpour, S.-H. Lee, H. Koo, S. Song, Y.-N. Kwon, S. H. Song, J. C. Bae, A. Jo, M.-J. Kwon, S. H. Han, S.-H. Kim, S. Hwang, M. L. Brongersma, *Science* **2020**, 370, 459.
- [284] M. A. Fusella, R. Saramak, R. Bushati, V. M. Menon, M. S. Weaver, N. J. Thompson, J. J. Brown, *Nature* **2020**, 585, 379.
- [285] A. Sourav, Z. Li, Z. Huang, V. D. Botcha, C. Hu, J.-P. Ao, Y. Peng, H.-C. Kuo, J. Wu, X. Liu, K.-W. Ang, *Adv. Opt. Mater.* **2018**, 6, 1800461.
- [286] J.-A. Huang, L.-B. Luo, *Adv. Opt. Mater.* **2018**, 6, 1701282.
- [287] K. Arora, D. P. Singh, P. Fischer, M. Kumar, *Adv. Opt. Mater.* **2020**, 8, 2000212.
- [288] P. Deshpande, P. Suri, H.-H. Jeong, P. Fischer, A. Ghosh, A. Ghosh, *J. Chem. Phys.* **2020**, 152, 044709.
- [289] W. R. Erwin, H. F. Zarick, E. M. Talbert, R. Bardhan, *Energy Environ. Sci.* **2016**, 9, 1577.
- [290] Z. Bao, N. Fu, Y. Qin, J. Lv, Y. Wang, J. He, Y. Hou, C. Jiao, D. Chen, Y. Wu, J. Dai, *ACS Appl. Mater. Interfaces* **2020**, 12, 538.
- [291] M. S. Mohamed Saheed, N. M. Mohamed, B. S. Mahinder Singh, R. Jose, *ACS Appl. Energy Mater.* **2019**, 2, 8707.
- [292] K. Xu, R. Zhou, K. Takei, M. Hong, *Adv. Sci.* **2019**, 6, 1900925.
- [293] M. Qiu, L. Zhang, Z. Tang, W. Jin, C.-W. Qiu, D. Y. Lei, *Adv. Funct. Mater.* **2018**, 28, 1803147.
- [294] Y. Gutiérrez, A. S. Brown, F. Moreno, M. Losurdo, *J. Appl. Phys.* **2020**, 128, 080901.
- [295] J. Xavier, S. Vincent, F. Meder, F. Vollmer, *Nanophotonics* **2018**, 7, 1.
- [296] Z. Li, J. Jin, F. Yang, N. Song, Y. Yin, *Nat. Commun.* **2020**, 11, 2883.
- [297] W. Wan, J. Gao, X. Yang, *Adv. Opt. Mater.* **2017**, 5, 1700541.
- [298] J. Li, S. Kamin, G. Zheng, F. Neubrech, S. Zhang, N. Liu, *Sci. Adv.* **2018**, 4, eaar6768.
- [299] F. Zhang, M. Pu, P. Gao, J. Jin, X. Li, Y. Guo, X. Ma, J. Luo, H. Yu, X. Luo, *Adv. Sci.* **2020**, 7, 1903156.
- [300] X. Duan, N. Liu, *ACS Nano* **2018**, 12, 8817.
- [301] J. Li, Y. Chen, Y. Hu, H. Duan, N. Liu, *ACS Nano* **2020**, 14, 7892.
- [302] I. Kim, G. Yoon, J. Jang, P. Genevet, K. T. Nam, J. Rho, *ACS Photonics* **2018**, 5, 3876.
- [303] S. Lee, K. Sim, S. Y. Moon, J. Choi, Y. Jeon, J.-M. Nam, S.-J. Park, *Adv. Mater.* **2021**, 33, 2007668.
- [304] K. S. Pasupuleti, M. Reddeppa, B.-G. Park, K. R. Peta, J.-E. Oh, S.-G. Kim, M.-D. Kim, *ACS Appl. Mater. Interfaces* **2020**, 12, 54181.
- [305] K. Xiong, O. Olsson, J. Sviridis, C. Palasingh, J. Baumberg, A. Dahlin, *Adv. Mater.* **2021**, 33, 2103217.
- [306] C. T. Cooper, M. Rodriguez, S. Blair, J. S. Shumaker-Parry, *J. Phys. Chem. C* **2014**, 118, 1167.
- [307] A. Fernandez-Bravo, D. Wang, E. S. Barnard, A. Teitelboim, C. Tajon, J. Guan, G. C. Schatz, B. E. Cohen, E. M. Chan, P. J. Schuck, T. W. Odom, *Nat. Mater.* **2019**, 18, 1172.
- [308] Y. Brasse, V. Gupta, H. C. T. Schollbach, M. Karg, T. A. F. König, A. Fery, *Adv. Mater. Interfaces* **2020**, 7, 1901678.
- [309] D. Wang, A. Yang, W. Wang, Y. Hua, R. D. Schaller, G. C. Schatz, T. W. Odom, *Nat. Nanotechnol.* **2017**, 12, 889.
- [310] R.-M. Ma, S.-Y. Wang, *Nanophotonics* **2021**, 10, 3623.
- [311] S. Zhang, X. Shi, S. Yan, X. Zhang, K. Ge, C. B. Han, T. Zhai, *ACS Sens.* **2021**, 6, 3416.
- [312] H. Xin, B. Namgung, L. P. Lee, *Nat. Rev. Mater.* **2018**, 3, 228.
- [313] N. L. Rosi, C. A. Mirkin, *Chem. Rev.* **2005**, 105, 1547.
- [314] S. Dutta, K. Saikia, P. Nath, *RSC Adv.* **2016**, 6, 21871.
- [315] S. H. Yun, S. J. J. Kwok, *Nat. Biomed. Eng.* **2017**, 1, 0008.
- [316] F. Soto, J. Wang, R. Ahmed, U. Demirci, *Adv. Sci.* **2020**, 7, 2002203.
- [317] Y. Ren, Q. Chen, M. He, X. Zhang, H. Qi, Y. Yan, *ACS Nano* **2021**, 15, 6105.
- [318] Y. Jin, *Adv. Mater.* **2012**, 24, 5153.
- [319] Y. Hong, D. Velegol, N. Chaturvedi, A. Sen, *Phys. Chem. Chem. Phys.* **2010**, 12, 1423.
- [320] T. L. H. Doan, N. X. D. Mai, K. Matsumoto, F. Tamanoi, *Enzymes* **2018**, 44, 61.
- [321] R. E. Yanes, J. Lu, F. Tamanoi, *Enzymes* **2012**, 32, 185.
- [322] D. Andren, D. G. Baranov, S. Jones, G. Volpe, R. Verre, M. Käll, *Nat. Nanotechnol.* **2021**, 16, 970.
- [323] R. Verre, L. Shao, N. O. Länk, P. Karpinski, A. B. Yankovich, T. J. Antosiewicz, E. Olsson, M. Käll, *Adv. Mater.* **2017**, 29, 1701352.
- [324] Y. Y. Tanaka, P. Albella, M. Rahmani, V. Giannini, S. A. Maier, T. Shimura, *Sci. Adv.* **2020**, 6, eabc3726.
- [325] J. T. Kim, U. Choudhury, H.-H. Jeong, P. Fischer, *Adv. Mater.* **2017**, 29, 1701024.
- [326] D. Schamel, A. G. Mark, J. G. Gibbs, C. Miksch, K. I. Morozov, A. M. Leshansky, P. Fischer, *ACS Nano* **2014**, 8, 8794.
- [327] Q. Xu, N. J. Boylan, J. S. Suk, Y.-Y. Wang, E. A. Nance, J.-C. Yang, P. J. McDonnell, R. A. Cone, E. J. Duh, J. Hanes, *J. Controlled Release* **2013**, 167, 76.
- [328] A. Tuteja, M. E. Mackay, S. Narayanan, S. Asokan, M. S. Wong, *Nano Lett.* **2007**, 7, 1276.
- [329] L. Lin, M. Wang, X. Peng, E. N. Lissek, Z. Mao, L. Scarabelli, E. Adkins, S. Coskun, H. E. Unalan, B. A. Korgel, L. M. Liz-Marzán, E.-L. Florin, Y. Zheng, *Nat. Photonics* **2018**, 12, 195.
- [330] E. Lee, D. Huang, T. Luo, *Nat. Commun.* **2020**, 11, 2404.
- [331] X.-Z. Chen, M. Hoop, F. Mushtaq, E. Siringil, C. Hu, B. J. Nelson, S. Pané, *Appl. Mater. Today* **2017**, 9, 37.
- [332] T.-Y. Huang, F. Qiu, H.-W. Tung, X.-B. Chen, B. J. Nelson, M. S. Sakar, *Appl. Phys. Lett.* **2014**, 105, 114102.
- [333] D. Walker, B. T. Käschorf, H.-H. Jeong, O. Lieleg, P. Fischer, *Sci. Adv.* **2015**, 1, e1500501.

- [334] D. Ahmed, T. Baasch, B. Jang, S. Pane, J. Dual, B. J. Nelson, *Nano Lett.* **2016**, *16*, 4968.
- [335] T. Xu, F. Soto, W. Gao, R. Dong, V. Garcia-Gradilla, E. Magaña, X. Zhang, J. Wang, *J. Am. Chem. Soc.* **2015**, *137*, 2163.
- [336] F. Soto, G. L. Wagner, V. Garcia-Gradilla, K. T. Gillespie, D. R. Lakshminpathy, E. Karshalev, C. Angell, Y. Chen, J. Wang, *Nanoscale* **2016**, *8*, 17788.
- [337] H. Joh, D. E. Fan, *Adv. Mater.* **2021**, *33*, 2101965.
- [338] S. Palagi, D. P. Singh, P. Fischer, *Adv. Opt. Mater.* **2019**, *7*, 1900370.
- [339] W. F. Paxton, K. C. Kistler, C. C. Olmeda, A. Sen, S. K. St. Angelo, Y. Cao, T. E. Mallouk, P. E. Lammert, V. H. Crespi, *J. Am. Chem. Soc.* **2004**, *126*, 13424.
- [340] W. F. Paxton, P. T. Baker, T. R. Kline, Y. Wang, T. E. Mallouk, A. Sen, *J. Am. Chem. Soc.* **2006**, *128*, 14881.
- [341] T.-C. Lee, M. Alarcón-Correa, C. Miksch, K. Hahn, J. G. Gibbs, P. Fischer, *Nano Lett.* **2014**, *14*, 2407.
- [342] D. Okawa, S. J. Pastine, A. Zettl, J. M. J. Fréchet, *J. Am. Chem. Soc.* **2009**, *131*, 5396.
- [343] J. K. G. Dhont, S. Wiegand, S. Duhr, D. Braun, *Langmuir* **2007**, *23*, 1674.
- [344] H. Eskandarloo, A. Kierulf, A. Abbaspourrad, *Nanoscale* **2017**, *9*, 12218.
- [345] D. Walker, M. Kübler, K. I. Morozov, P. Fischer, A. M. Leshansky, *Nano Lett.* **2015**, *15*, 4412.
- [346] M. Pal, N. Somalwar, A. Singh, R. Bhat, S. M. Eswarappa, D. K. Saini, A. Ghosh, *Adv. Mater.* **2018**, *30*, 1800429.
- [347] S. Wilhelm, A. J. Tavares, Q. Dai, S. Ohta, J. Audet, H. F. Dvorak, W. C. W. Chan, *Nat. Rev. Mater.* **2016**, *1*, 16014.
- [348] C. Reich, I. Tinoco Jr., *Biopolymers* **1980**, *19*, 833.
- [349] C. Merten, T. P. Golub, N. M. Kreienborg, *J. Org. Chem.* **2019**, *84*, 8797.
- [350] L. A. Nafie, in *Vibrational Optical Activity: Principles and Applications*, Wiley, Hoboken, NJ, USA **2011**.
- [351] M. Kuwata-Gonokami, N. Saito, Y. Ino, M. Kauranen, K. Jefimovs, T. Vallius, J. Turunen, Y. Svirko, *Phys. Rev. Lett.* **2005**, *95*, 227401.
- [352] V. K. Valev, N. Smisdom, A. V. Silhanek, B. De Clercq, W. Gillijns, M. Ameloot, V. V. Moshchalkov, T. Verbiest, *Nano Lett.* **2009**, *9*, 3945.
- [353] Y. Zhao, L. Xu, W. Ma, L. Wang, H. Kuang, C. Xu, N. A. Kotov, *Nano Lett.* **2014**, *14*, 3908.
- [354] A. O. Govorov, Z. Fan, P. Hernandez, J. M. Slocik, R. R. Naik, *Nano Lett.* **2010**, *10*, 1374.
- [355] M. H. Alizadeh, B. M. Reinhard, *ACS Photonics* **2015**, *2*, 942.
- [356] M. Schäferling, D. Dregely, M. Hentschel, H. Giessen, *Phys. Rev. X* **2012**, *2*, 031010.
- [357] M. Hentschel, M. Schäferling, X. Duan, H. Giessen, N. Liu, *Sci. Adv.* **2017**, *3*, e1602735.
- [358] M. Schäferling, *Chiral Nanophotonics*, Springer Series in Optical Sciences, Vol. 205, Springer International Publishing, New York **2017**, pp. 43–60.
- [359] S. Both, M. Schäferling, F. Sterl, E. A. Muljarov, H. Giessen, T. Weiss, *ACS Nano* **2022**, *16*, 2822.
- [360] K. W. Smith, H. Zhao, H. Zhang, A. Sánchez-Iglesias, M. Grzelczak, Y. Wang, W.-S. Chang, P. Nordlander, L. M. Liz-Marzán, S. Link, *ACS Nano* **2016**, *10*, 6180.
- [361] L.-Y. Wang, K. W. Smith, S. Dominguez-Medina, N. Moody, J. M. Olson, H. Zhang, W.-S. Chang, N. Kotov, S. Link, *ACS Photonics* **2015**, *2*, 1602.
- [362] C. Bustamante, M. F. Maestre, I. Tinoco Jr., *J. Chem. Phys.* **1980**, *73*, 4273.
- [363] J. Karst, N. H. Cho, H. Kim, H.-E. Lee, K. T. Nam, H. Giessen, M. Hentschel, *ACS Nano* **2019**, *13*, 8659.
- [364] P. Woźniak, I. De Leon, K. Höflich, C. Haverkamp, S. Christiansen, G. Leuchs, P. Banzer, *Opt. Express* **2018**, *26*, 19275.
- [365] O. Arteaga, J. Sancho-Parramon, S. Nichols, B. M. Maoz, A. Canillas, S. Bosch, G. Markovich, B. Kahr, *Opt. Express* **2016**, *24*, 2242.
- [366] D. C. Hooper, A. G. Mark, C. Kuppe, J. T. Collins, P. Fischer, V. K. Valev, *Adv. Mater.* **2017**, *29*, 1605110.
- [367] D. L. Andrews, T. Thirunamachandran, *J. Chem. Phys.* **1979**, *70*, 1027.
- [368] P. Fischer, F. Hache, *Chirality* **2005**, *17*, 421.
- [369] T. Petralli-Mallow, T. M. Wong, J. D. Byers, H. I. Yee, J. M. Hicks, *J. Phys. Chem.* **1993**, *97*, 1383.
- [370] H. J. Singh, Saumitra, V. R. Singh, S. K. Sikdar, B. Jayaprakash, A. Ghosh, *ACS Photonics* **2016**, *3*, 863.
- [371] H.-N. Barad, M. Alarcón-Correa, G. Salinas, E. Oren, F. Peter, A. Kuhn, P. Fischer, *Mater. Today* **2021**, *50*, 89.



Jang-Hwan Han is a postdoctoral fellow at the Gwangju Institute of Science and Technology (GIST). He received an M.Sc. in information and communication engineering from Inha University and a Ph.D. in materials science and engineering from GIST. During his Ph.D., he developed magnetically active optoelectronic devices including light-emitting diodes, photovoltaics, displays, and sensors. He has recently expanded his research domain into nanophotonic devices for active metamaterials, plasmonic display, and nanorobotic applications.



Doeun Kim is a Ph.D. student at the School of Electrical Engineering and Computer Science, Gwangju Institute of Science and Technology (GIST). She received a B.Eng. and M.Eng. in materials engineering and convergence technology from Gyeongsang National University (GNU). She was an assistant researcher at the Electronic Convergence Materials Division, Korea Institute of Ceramic Engineering and Technology (KICET) for 3 years. Her research interests include 3D nanofabrication, biophotonic metasurfaces and metamaterials, and super hydrophobicity.



Juhwan Kim is a M.Sc./Ph.D. student at the School of Electrical Engineering and Computer Science, Gwangju Institute of Science and Technology (GIST). He received a B.Sc. in physics from GIST in 2022. He has research interests including chiral plasmonics and plasmonic sensing.



Gyurin Kim is a M.Sc./Ph.D. student at the School of Electrical Engineering and Computer Science, Gwangju Institute of Science and Technology (GIST). He received a B.Sc. in electrical engineering and computer science from GIST in 2021. He has research interests including 3D nanofabrication, plasmonic sensing, and active metamaterials.



Peer Fischer is a professor at the University of Stuttgart and he heads the independent Micro Nano and Molecular Systems Lab at the Max Planck Institute for Intelligent Systems. He received a B.Sc. in physics from Imperial College London and a Ph.D. from the University of Cambridge. He was a NATO postdoctoral fellow at Cornell, and a Rowland Fellow at Harvard. In 2009, he received an Attract Award from the Fraunhofer Society. He won two ERC Grants and a World Technology Award. He is on the editorial board of Science Robotics and a fellow of the Royal Society of Chemistry.



Hyeon-Ho Jeong is an assistant professor at the Gwangju Institute of Science and Technology (GIST). He received B.Eng. and M.Eng. in electrical engineering from Dankook University and a Ph.D. in materials engineering from Max Planck Institute for Intelligent Systems and EPFL. Before joining the GIST, he was a research associate at the Cavendish Laboratory, the University of Cambridge for 1.5 years. He was awarded the Graduate Student Awards in 2016 from MRS (Gold) and in 2017 from EMRS for research in the field of material science. He has research interests including micro and nano robotics, chirality, plasmonics, and metamaterials.